AFRL-WS-WP-TR-2000-9001

TECHNOLOGY HORIZONS
SELECTED SCIENCE AND TECHNOLOGY ARTICLES

AIR FORCE RESEARCH LABORATORY
TECH CONNECT
1864 4TH STREET, SUITE 1
WPAFB OH 45433-7131

MARCH 2000

AIR FORCE RESEARCH LABORATORY
AIR FORCE MATERIEL COMMAND
WRIGHT-PATTERSON AIR FORCE BASE, OH 45433

REPORT DOCUMENTATION PAGE	Form Approved OMB No. 0704-0188

1. AGENCY USE ONLY *(Leave blank)*	2. REPORT DATE	3. REPORT TYPE AND DATES COVERED
	MARCH 2000	Final MARCH 2000

4. TITLE AND SUBTITLE
TECHNOLOGY HORIZONS
SELECTED SCIENCE AND TECHNOLOGY ARTICLES

5. FUNDING NUMBERS

6. AUTHOR(S)

7. PERFORMING ORGANIZATION NAME(S) AND ADDRESS(ES)

TECH CONNECT
1864 4TH STREET, SUITE 1
WPAFB OH 45433-7131

8. PERFORMING ORGANIZATION REPORT NUMBER

9. SPONSORING/MONITORING AGENCY NAME(S) AND ADDRESS(ES)

AIR FORCE RESEARCH LABORATORY
AIR FORCE MATERIEL COMMAND
WRIGHT-PATTERSON AFB OH 45433-7101

10. SPONSORING/MONITORING AGENCY REPORT NUMBER

AFRL-WS-WP-TR-2000-9001

11. SUPPLEMENTARY NOTES

12a. DISTRIBUTION AVAILABILITY STATEMENT

PUBLIC RELEASE; DISTRIBUTION UNLIMITED.

12b. DISTRIBUTION CODE

13. ABSTRACT *(Maximum 200 words)*

Human Effectiveness Directorate: Networked-Enabled Image Generators in a Distributed Interactive Simulation and High Level Architecture Environment. Information Directorate: Methods for Detecting Tampering in Digital Images and Optical Redundant Array of Inexpensive Drives. Materials and Manufacturing: Waterjet Technology Used in Green Munitions Program. Air Force Office of Scientific Research: Dip-Pen Nanolithography, "Perfect" Mirror Design Technology, and "Stress Check" for Composite Bonded Aircraft Structures. Propulsion Directorate: Additive Improvements Performance of Heating/Cooling Systems. Sensors Directorate: Higher Operating Temperature for Ultra-High Density Optical and Optical Limiting In Hydrothermal Zinc Oxide Crystals. Air Vehicle Directorate: Active Core Exhaust Control and First Flight Test Demonstration of Neural Network Software. Space Vehicles Directorate: Treacherous High Ground: The Near Earth Space Environment. Directed Energy Directorate: Biophotonics Applications Of High-Power Semiconductor Diode Laser Technology.

14. SUBJECT TERMS	15. NUMBER OF PAGES
	52
	16. PRICE CODE

17. SECURITY CLASSIFICATION OF REPORT	18. SECURITY CLASSIFICATION OF THIS PAGE	19. SECURITY CLASSIFICATION OF ABSTRACT	20. LIMITATION OF ABSTRACT
UNCLASSIFIED	UNCLASSIFIED	UNCLASSIFIED	SAR

Standard Form 298 (Rev. 2-89) (EG)
Prescribed by ANSI Std. 239.18
Designed using Perform Pro, WHS/DIOR, Oct 94

INTRODUCTION

AFRL Technology Horizons selected science and technology articles derived from the research and development activities of the Air Force Research Laboratory. These articles contain information considered likely to be transferable across industrial, regional, or disciplinary lines and are issued to encourage commercial applications.

Availability of AFRL Science and Technology Articles And Technical Support Packages

Distribution of AFRL Science and Technology Articles, a quarterly publication, is limited to scientists and engineers in Government and U.S. Industry and to other domestic technology transfer agents. Request for individual articles or for Technical Support Packages announced herein should be addressed to:

Air Force Research Laboratory
ATTN: TECH CONNECT
1864 4th Street, Suite 1
Wright-Patterson AFB OH 45433-7131

Please reference the six-digit document number located at the end of each article. Additional information on the Air Force Research Laboratory can be obtained from the same office.

TABLE OF CONTENTS

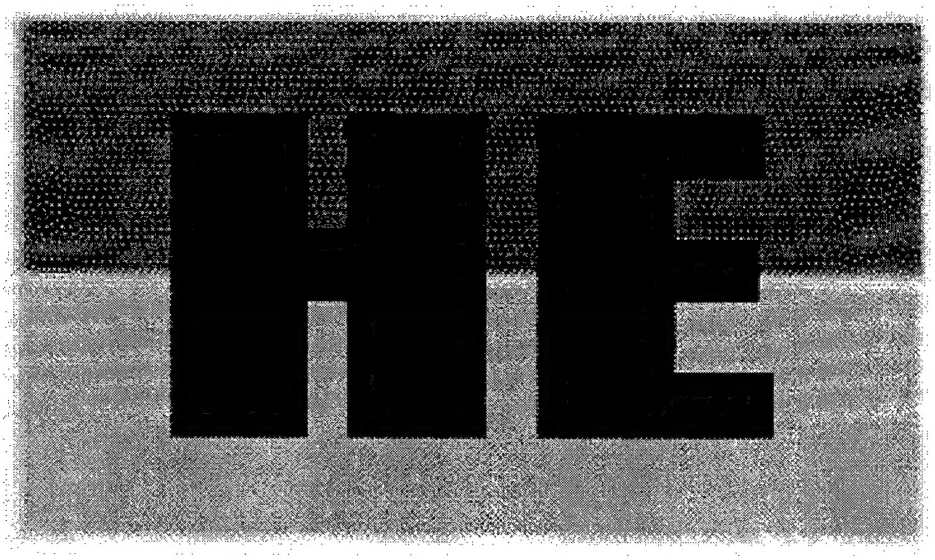

Human Effectiveness Directorate

Network-Enabled Image Generators in a Distributed Interactive Simulation and High Level Architecture Environment

Network-enabled image generators reduce integration time and maintenance costs while increasing the consistency of presentation in the visual scene.

AFRL's Human Effectiveness Directorate, Warfighter Training Research Division, Mesa, AZ.

A number of substantial technology advancements will greatly improve flight simulator training in the future. New technologies combined with developments in interactive simulation communication protocols, such as Distributed Interactive Simulation (DIS) and High Level Architecture (HLA), have pushed flight simulator training possibilities to a new level. The Human Effectiveness Directorate developed a concept of Distributed Mission Training (DMT) which is a shared training environment comprised of live, virtual, and constructive simulations allowing warfighters to train individually or collectively at all levels of war. DMT allows multiple players at multiple sites to engage in training scenarios ranging from individual and team participation up to full theater-level battles. It allows participation, using almost any type of networkable training device, from each weapon system and mission area. Additionally, computer-generated or constructive forces can be used to substantially enhance the scenario. The quality of the Image Generators (IGs) used in these devices are key to their success. However, current methods for integrating hosts and IGs are not standardized, making it difficult to upgrade IGs.

The traditional way for a host simulator to connect to an IG is by using an Interface Control Document (ICD) provided by each IG manufacturer. Each connection between a host and an IG requires a custom software integration, usually done by the host, to conform to the IG's ICD. Thus, the host-IG integration is the responsibility of the host with implementation often very host specific. The stand-alone host creates all simulation information.

With the advent of common network standards, such as DIS and HLA, that allow various simulators to be interconnected, simulation information is generated from multiple host simulators and shared over a public network.

Conceptually, the IG should know the visualized environment of the virtual world independent of the host, while the host controls the positioning of the viewpoint in the virtual world. With its own network interface unit (NIU) or visual interface unit (VIU), the IG could access the public DIS/HLA network directly and also have access to all network data without translation. The host, in-turn, would only need to tell the IG the view of the world to show.

The Human Effectiveness Directorate experimented with an IG connected solely to a public DIS network. Informal tests were performed using DIS with various error thresholds (with and without smoothing) to see if an IG connected only to the public network would be sufficient. The results were only acceptable when the data was sent out essentially frame-by-frame. However, this quickly flooded the public network with data and was therefore unacceptable.

The IG often needs to provide specific data exclusively to the host. Based on the results of the experiment, adding this information would increase the public network load and the need for two networks becomes apparent. A combination of one public network, from which the IG gets most of its data, and one private network, over which the host and IG communicate frame-by-frame in order to reduce latency and reduce public network bandwidth requirements, appears to be the most effective configuration. A schematic of the network is shown in Figure 1.

The change from standalone hosts to distributed simulations connected over a public network has changed the way IGs and hosts relate. With most of the information about the virtual world existing on some type of public DIS/HLA network, it makes sense for IGs to become "network-enabled", accessing information directly, and simplifying the host IG interface to the most basic information. This basic information may be more easily standardized than a full traditional ICD.

Since a network-enabled IG gets most of its information from the public DIS/HLA network, the information required from the host is greatly simplified. The Human Effectiveness Directorate is developing a standard open system architecture IG protocol interface that defines the formats of the data sent or received from a network-enabled IG. The protocol is kept simple by only supporting network-enabled IGs.

This protocol would allow IGs to be "plug and play" for hosts that have a standard IG interface capability. Since most of the information comes from the public network, the time to integrate an IG with a new host should be significantly shortened. Visualization on a particular IG may be more uniform across different applications. Different IGs could be con-

nected to a host without modification to the host for IG replacements or upgrades.

A network-enabled IG that supports both DIS and HLA would allow IG manufacturers the opportunity to specify the data they would like to see on the public network (i.e., weather, dynamic terrain, and time of day) and then have direct access to that data rather than relying on integrators to pass that data through their simulations. This allows for a more correlated picture and avoids passing unneeded information through the host. This configuration also helps ensure the availability of the information needed for an IG.

The use of a standard IG protocol with a network-enabled IG promotes the possibility of a "plug-and-play" IG. This will allow IGs to be changed and upgraded more easily than currently possible and allow hosts to take advantage of the rapidly improving capabilities of new IGs.

This article was written by Mr. Lance R. Call (Raytheon) of the Air Force Research Laboratory's Human Effectiveness Directorate. For more information contact TECH CONNECT at 1-800-203-6451 or visit the web site at http://www.afrl.af.mil (Technology Transfer). Reference Document HE-99-05.

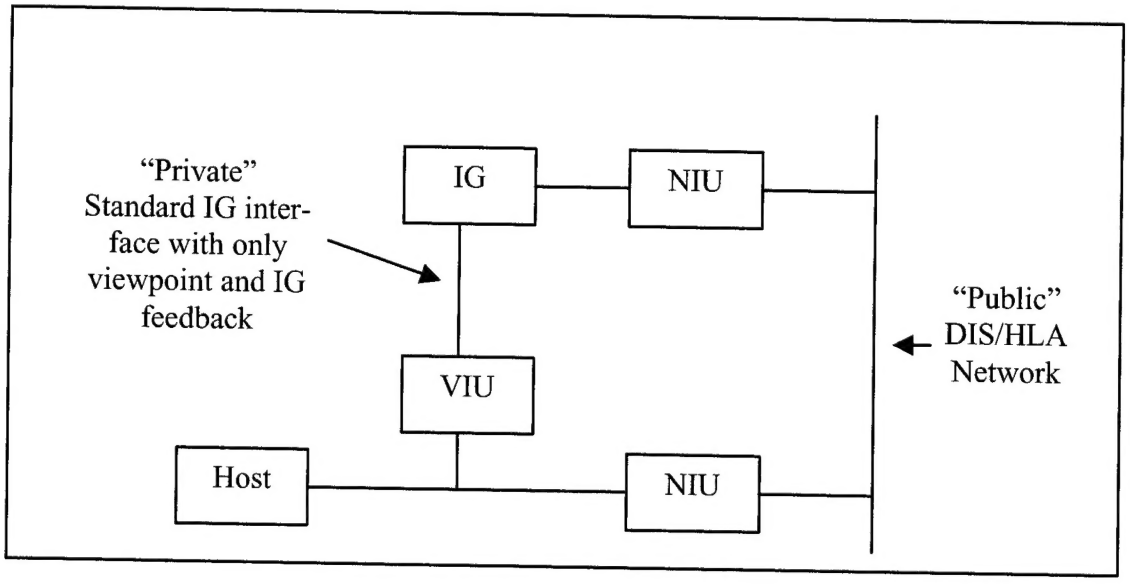

Figure 1. Network-enabled IG

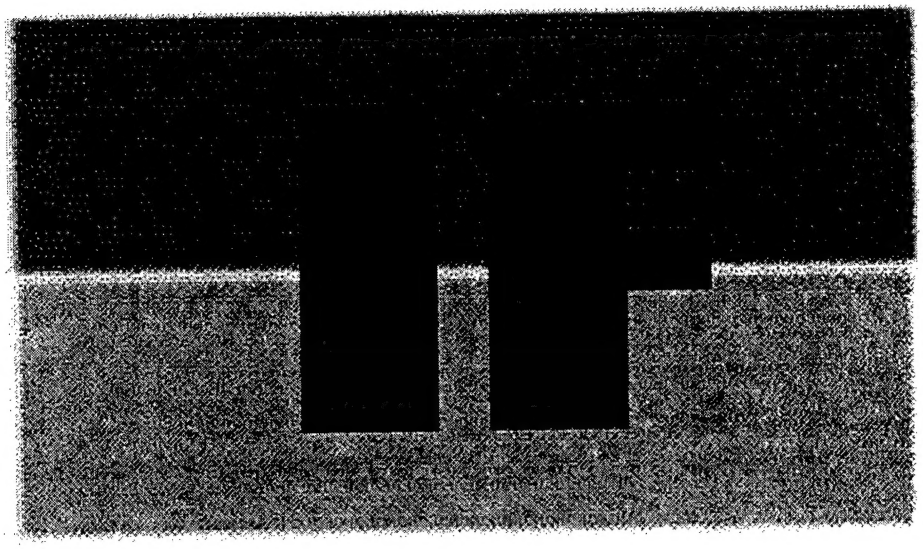

Information Directorate

Methods for Detecting Tampering in Digital Images

New methods for identifying and authenticating tampering in digital images.

AFRL's Information Directorate, Information and Intelligence Exploitation Division, Multi-Sensor Exploitation Branch, Rome, NY.

The use of digital images is becoming more prevalent, from taking pictures with a digital camera to using satellite imagery to track military targets in Kosovo. With this increased reliance on digital images for information, the need to ensure their authenticity increases as well.

Existing digital imagery authentication techniques are based on cryptographic principles and digital signatures. These schemes effectively protect the data from modification during transmission, but they offer no protection following transmission. Since the information needed for these schemes to perform the authentication is separate from the data, an attacker can simply modify the data, recalculate the new message digest or digital signature, and attach them together. Without knowledge of the original data or of the original authentication information, it is impossible to contest the authenticity of the modified digital image. However, since the value of digital images is based on its content, the image bits can be modified to embed codes without changing the meaning of its content. Once the codes are embedded in the data content and the data is manipulated, these codes will also be modified so the authenticator can examine them to verify the integrity of the data.

One approach to verify an image's authenticity is to embed checksums into the least significant bits (LSB) of the image. A secret numeric key known by both the sender and the recipient protects these checksums. Walton[1] proposes a technique that uses a key-dependent pseudo-random walk on the image. The checksum is obtained by summing the numbers determined by the seven most significant bits and taking a remainder operation with a large integer *L*. The checksum is inserted in binary form in the least significant bit of selected pixels. This could be repeated for many disjoint random walks or for one random walk that goes through all pixels. The method is very fast and often modifies only half of the pixels by one gray level, which is undetectable to the human eye.

Although the LSBs of the image are disturbed, the resulting image is perceptually equivalent to the original. The human eye cannot detect any difference because changes to the LSB of a pixel affect its value by only one. Since pixel values range from 1 to 256, there will be at most a $\pm 1/256$ change (±0.39%) in pixel intensity. This is important since the intent is to minimize the degradation of image fidelity during the embedding procedure. This article extends Walton's algorithm to allow one to localize the tampering.

The algorithm for embedding a checksum is outlined by Walton in three steps. The use of this algorithm is varied, as reported in this article, to achieve different results, but the embedding process is the same throughout. To embed a checksum, start with a $M \times N$ matrix of pixel values that will be used for embedding.

Walton's steps for embedding are:

(1) use the user-specified key to determine the random walk over the matrix,

(2) go over the entire matrix to construct the checksum out of the seven most-significant bits of each pixel, and

(3) embed the checksum bits, one by one, into the pixels at the random-walk addresses.

To extract the checksum and check for authenticity:

(1) use the user-specified key to determine the random walk over the matrix,

(2) go over the entire matrix to construct a checksum out of the seven most-significant bits of each pixel, and

(3) use the random-walk addresses and assemble the checksum from the LSBs of the visited pixels that will be compared with the checksum obtained in step two.

There are three different implementations to this basic algorithm. The first version, named "Build One," protects the entire image with one checksum and can determine whether the image was tampered. The second version, "Build Two," embeds checksums into sub-blocks of a grayscale image in order to localize tampering. The last version, "Build Three," extends Build Two to deal with color Red, Green, Blue (RGB) images and implements a walk-dependent checksum. A walk-dependent checksum prevents tampering based on exchanging groups of pixels with the same checksum or exchanging sub-blocks with their embedded checksums. Rather than obtain the checksum from summing the pixel values, multiply the pixel value by a function of the position of that pixel, and then sum these products.

Build One takes a $M \times N$ grayscale image and a numeric key and embeds a single checksum into the image. Since every pixel in the image is used to create the

32-bit checksum, the whole image is protected. Although 32 pixels (maximum) will be modified by one grayscale level (maximum), any minute tampering on the image can be detected. Because the checksum, *CS*, is computed from summing the pixel values throughout the whole image (Equation 1), modifying the image will invalidate the checksum.

Equation 1:

$$CS_{32-bit} = \sum_{i,j} (p_{i,j})$$

where

$CS_{32\text{-bit}}$ = 32-bit checksum number
$p_{i,j}$ = pixel value at position (i, j)

Output is one of the following two messages:

"Your image file most likely has not been tampered with."

or

"Your image file has been tampered with!"

The authenticator either signifies the image has been tampered with or has not likely been tampered with. The quantifier "most likely" points to a weakness of this scheme. A successful attack on this scheme is to exchange pixels in the image. Exchanging pixels, provided the pixels containing the checksum are not touched, will not affect the checksum, and therefore, this form of tampering would not be detected.

Build One attempts to protect every pixel in the image with a single checksum, no matter what the dimensions of the image are. Although it may be able to detect tampering, it cannot give any indication as to the tampered location in the image.

Build Two embeds multiple checksums into an image in order to localize any tampering. Build Two takes a $M \times N$ grayscale image, and a numeric key, and also allows the user to specify a block size B. The image is broken up into $B \times B$ sub-blocks, each embedded with a checksum.

Since the image will be broken into square blocks, the only way to protect every pixel is to have an image with a length and width that are multiples of the block size chosen. For example, if an image is 125 pixels wide and the specified block size is 30, the last five-pixel columns will be unprotected. If the size of the image is known and the block size is chosen appropriately, the number of unprotected pixels can be kept to a minimum. If it is crucial to protect all pixels, an algorithm must be devised for these leftover blocks.

The smallest block size used has sides that are six pixels long. There are 36 pixels in this block and at least 32 pixels are needed to embed the 32-bit checksum.

When Build Two checks for authenticity, any block without matching checksums is marked with a black X and a white border. This strategy allows a tampered block to be noticed, regardless of the background color.

The following figures give an example of Build Two. In Figure 1, an original aerial photograph of an Army Urban Training Site near Fort Drum, New York is shown. Figure 2 shows the image after the checksums have been embedded into sub-blocks (every 6x6 block of pixels) of the image. It is impossible for human eyes to detect the difference between the two. Figure 3 gives an example of a tampered version of the image. Figure 4 shows the receiver's view after the image undergoes the tamper (checksum extraction) test. Any tampered blocks are marked.

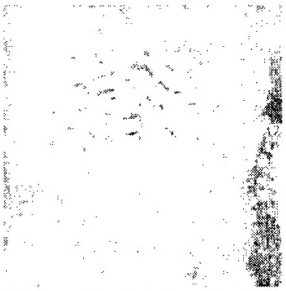

Figure 1. Original image.

Figure 2. 'Protected' image.

Figure 3. Tampered image.

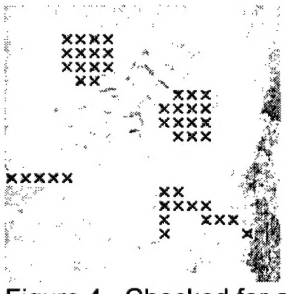

Figure 4. Checked for authenticity.

Build Two is able to localize and mark the tampered areas. The smaller the chosen block size, the more precise the algorithm can pinpoint areas in an image. The price for this greater accuracy, however, is performance. The smaller the block size, the more checksums to calculate and embed, and consequently, the

longer it would take to verify the image's authenticity. Performance varies inversely with the size of the blocks.

During initial testing, some blocks were reported as tampered even when the image had not been touched. This was due to the boundary conditions imposed by MATLAB's representation of intensity value. To solve the problem, the image was normalized to [0,255] instead of using MATLAB's range of [1,256]. This normalization, performed before embedding and extracting, ensured correct encoding of the LSB.

The weaknesses of Build Two is similar to the weaknesses of Build One. Exchanging pixels in each sub-block will not be detected. Moreover, exchanging sub-blocks will also be undetectable. To overcome these weaknesses, the embedded checksum must be walk-dependent.

Build Three extends Build Two to deal with RGB (color) images and introduces a walk-dependant checksum. The walk-dependant checksum of Build Three does not allow pixels or blocks to be exchanged without detection, which is a weakness of the previous two Builds. Build Three calculates the checksum by multiplying the pixel values by a function of their positions, and then summing them (Equation 2).

Equation 2:

$$CS_{32-bit} = \sum_{i,j} \left(p_{i,j} * f(i,j) \right)$$

where

$CS_{32\text{-bit}}$ = 32-bit checksum number
$p_{i,j}$ = pixel value at position (i, j)
$f(i,j)$ = function of i and j

Since an RGB image is structured like three grayscale images on top of each other (a $M \times N$ matrix for each RGB level), there are more checksums embedded in the RGB image. Consequently, performance suffers. If the same size image and block size are used for a grayscale and an RGB image, the RGB version would embed three times as many checksums as the grayscale because it embeds them into each RGB level separately. The trade-off is that modifications localized to a single color plane can be detected.

The following figures are the results of using Build Three to embed checksums into every 12×12 block of pixels of a test image. Figure 5 shows the original image, while Figure 6 shows the image with the embedded checksum. Figure 7 shows the image after some minor modifications were made. Figure 8 shows the results of using the authentication algorithm. Any tampered areas were highlighted to make the changes obvious.

Figure 5. Original image.

Figure 6. 'Protected' image.

Figure 7. Tampered image.

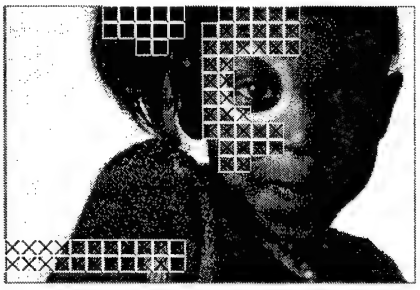

Figure 8. Checked for authenticity.

Since each of the three levels of RGB images are embedded with a checksum in Build Three, it is possible to detect minute changes in just one of the color levels. Figures 9, 10A, and 10B demonstrate this capability. The original image was modified in three areas. In each area, a different color plane was slightly modified to produce the tampered image. Although the modifications are imperceivable by the human eye, the implemented algorithm was able to successfully localize the changes (see Figures 10A and 10B).

Figure 9. Original image.

Figure 10A. Tampered image.

Figure 10B. Checked for authenticity.

With the increased reliance on images for information, it is very important to protect digital images from unauthorized modification. The proposed algorithm checks for and localizes any tampering to a digital image.

All three previous Builds work well for detecting any modification to an image. However, because these algorithms are based on modifying the LSBs, they cannot distinguish between malicious and non-malicious attacks on a digital image. Malicious attacks are attacks that modify the content of an image including manipulation, deletion, or addition of features. Non-malicious attacks modify the pixel values of an image, but do not modify its contents. Examples of non-malicious attacks are adjustment of brightness or contrast, lossy compression, or filtering. An acceptable content authentication scheme should protect all pixels in an image and distinguish between non-malicious and malicious changes to digital images.

One possible approach to solve the malicious/non-malicious weakness of the previous Builds is to embed watermarks in the frequency domain rather than in the LSB's of pixels. Frequency domain techniques generally provide more robustness with respect to most of the signal processing attacks. LSB embedding techniques, although easy to implement, are too fragile for content authentication purposes.

Another approach is to embed the checksum into a more significant bit-plane (i.e. the third or fourth bit). With this approach, the image would be less sensitive to minor changes, such as adding noise. M-sequences could also be embedded into the image instead of a checksum, as proposed by van Schyndel, Tirkel, and Osborne[2]. With embedded m-sequences, a correlation detector is used to determine whether an image (or black) has been tampered.

REFERENCES

[1] S. Walton, "Information Authentication for a Slippery New Age," *Dr. Dobbs Journal*, April 1995, Vol. 20, No. 4, pp. 18-26.

[2] R. G. van Schyndel, A. Z. Tirkel, and C. F. Osborne, "A digital watermark," *Proc. of the IEEE International Conference on Image Processing*, November 1994, Vol. 2, pp. 86–90.

This article was written by 1Lt Arnold Baldoza and Mr. Michael Sieffert of the Air Force Research Laboratory's Information Directorate. For more information contact TECH CONNECT at 1-800-203-6451 or visit the web site at http://www/afrl.af.mil (Technology Transfer). Reference document IF-99-05.

Optical Redundant Array of Inexpensive Drives

New storage technology goes operational.

AFRL's Information Directorate, Information and Intelligence Exploitation Division, Global Information Base Branch, Rome, NY.

The Information Directorate has pioneered research into the development of advanced, high-performance storage technology for next-generation computer systems. The Global Information Base Branch successfully installed a new computer storage device, developed by Rising Edge Technologies, Inc., in Osan AB, Korea. Working closely with the customer, U.S. Forces Korea (USFK), a total turnkey solution was conceived. The storage device is operational on a classified data network that is readily accessed by both the U.S. and Republic of Korea (ROK) forces. The heart of the solution is a storage device developed under AFRL's Advanced Development Program. The original program was called Optical Redundant Array of Inexpensive Drives (O-RAID).

Recent developments in volumetric memories offer quantum leaps in capacity, throughput rates and access times. Concepts in holographic storage, two photon absorption, bacteriorhodopsin, synthetic DNA, and magnetic nanotechnology are being exploited by the Information Directorate to meet the various hierarchical demands for computer storage. Predictions of terabit per cubic centimeter storage capacities, at gigabit per second data rates and nanosecond access times, are now being validated. Research and development programs in progress indicate that these goals can be exceeded. The emerging technologies of "free space" optical interconnects, associative retrieval, and field programmable gate arrays are being integrated to develop a "smart memory" for associative retrieval, which will be able to perform change detection by fusing data from a number of complimentary sensors. Rather than transmit a continuous data stream, it communicates only the sensor's change (i.e., it uses a "cognitive" bandwidth).

The storage technology leverages commercial off-the-shelf components to assemble a fault-tolerant storage device that readily attaches to standard computers and data networks. Fault-tolerance enables USFK to protect mission-critical data. The parallel system design provides for greater on-line storage and faster data access speeds. The ability to remove the storage disk media provides for safe storage of classified data.

The Information Directorate also configured a web-based server on a Dell workstation running Windows NT™, which improved user access to classified data by both the U.S. and ROK forces with minimal user training. The Directorate also investigated the potential of installing new software on the server to perform language translation. USFK has a need to translate documents from English to Hangul (Korean language). The entire system installation, test and user training was completed in approximately two weeks.

This article was written by Mr. Fred Haritatos of the Air Force Research Laboratory's Information Directorate. For more information contact TECH CONNECT at 1-800-203-6451 or visit the web site at http://www.afrl.af.mil (Technology Transfer). Reference document IF-99-04.

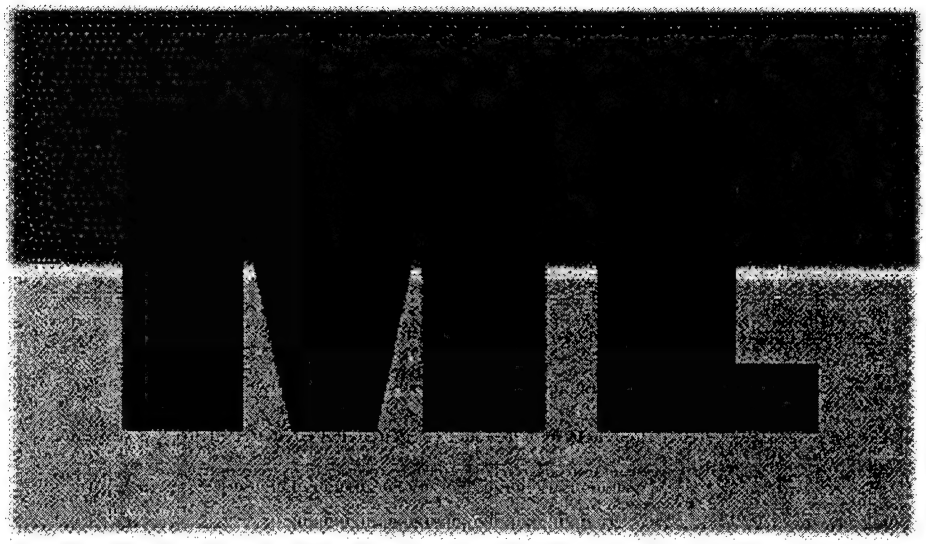

Materials and Manufacturing Directorate

Innovations in Materials Design

Computational approach to the design/discovery of new materials.

AFRL's Materials and Manufacturing Directorate, Manufacturing Technology Division, Materials Process Design Branch, Wright-Patterson AFB, OH.

Scientists in the Materials and Manufacturing Directorate, interested in seeking a computational approach to predicting the existence of a multi-element compound, sponsored a collaborative research effort, which led to a significant breakthrough in using neural networks to help design new materials. This effort resulted in the discovery that a nonlinear expression involving an elementary material property could be used to predict, with greater than 99 percent accuracy, the existence of a compound for a multi-element materials system. This discovery will result in significant time and resource savings and will speed the search for future useful materials.

For purposes of discussion, consider the subset of inorganic compounds. Simply deriving the possible number of binary, ternary and quaternary combinations of the known stable elements (roughly 100) would lead to the observation that there are about 5,000 binaries, 162,000 ternaries and 4,000,000 quaternaries possible (i.e., without considering multiple stoichiometries). Many of these combinations do not form compounds. Based upon conservative efforts, those that do form compounds contain data which exist for about 80% (over 4000) of the binary systems, 5% (about 8000) of the ternary systems, and less than 0.1% (nearly 4000 - when including oxides and halides) of the quaternary systems. By combining the number of compounds and solutions having distinct properties, which are both stable and producible, it is conceivable that the total number of useful material systems is in the billions. This article addresses exploration of more efficient methods to organize material systems data using both supervised and unsupervised artificial neural networks.

A principal driver for scientific and engineering endeavors is the 'mapping' of materials information (i.e., the mapping of structure, to properties, processing & use conditions). From Mendeleev and the 'Periodic Table' to present day electronic databases, the impetus to organize vast amounts of continually evolving materials data is increasingly driven by a globally competitive marketplace and 'atomic-scale' precision in the quality of information. For millennia, materials have been developed through the empirical correlation of processing and properties, and the role of materials science has been primarily one of explaining observed behavior and phenomena from experimentation and/or computational models. However, with today's increasing cost of experimentation and decreasing cost of computation, a clear motivation exists for a materials design and/or discovery approach which exploit science-based models validated with a minimum number of experiments.

An expanse of computational methods, ranging from *ab initio* to constitutive and even qualitative or semi-empirical models of materials and their associated mappings, is available. Given the enormity of the data-space to be considered, there is obvious benefit in the synergistic use of multiple methods. In the last millennia there has been a significant number of achievements in the development of materials science, chemistry, and physics (experimental and theoretical). However, the most difficult problem - calculating the intrinsic properties of multi-element compounds from the knowledge of their constituent element properties - remains unsolved. As elemental and compound materials data have become more prevalent, so has the impetus to develop accurate and expeditious methods of prediction. This evolving, but converging, focus on methods is also being driven by computing technology and a 'web-based' community of informed physicists, chemists, and materials researchers who are keenly aware of the potential rewards for innovation in materials design and discovery.

The prediction of new materials and their properties, in theory, is believed to be a completely straightforward problem. The fundamental equations of quantum mechanics for solids are well established and can be numerically solved, at least approximately, by powerful 'first-principles' based methods developed over the last decade. Yet, in practice, the typical approach is to establish 'easy-to-apply' rules for screening large numbers of candidate stoichiometries, which may or may not be known compounds. One reason for such practice, in lieu of computation, is that although atomic interactions regarding intermetallic compounds are well understood, it is not an easy task to evaluate the total energy of solids. The energy of an isolated atom is on the order of 10^6 eV, while the interatomic cohesive energy is on the order of 1-10 eV/atom. Thus, a method that is accurate to one part in 10^6 or better is applied. The other fact that greatly complicates evaluating the cohesive energy by theoretical methods is the number of particles involved (i.e., given a macroscopic solid having properties represen-

tative of bulk material), which may exceed 10^{23} nuclei and electrons.

In view of these considerations, a "direct" computational approach to predicting the properties of bulk macroscopic matter is generally not practical. When the system relaxation times are fast (10^{-12} seconds) and periodic boundary conditions can be applied with confidence, then it is possible to model the equation of state with high accuracy. In general, however, there is a need to simulate much larger numbers of molecules over longer time frames. The fundamental difficulty is that the number of particles treated as small is of the order of 10^6, and the time step that must be used to conserve energy is of the order of 10^{-15} seconds. Macroscopic matter will contain at least hundreds of millions of particles and many of the fastest relaxation processes are slower than the millisecond regime. Clearly, those physical properties dependent upon integrals of long range correlation functions cannot be calculated with sufficient accuracy nor can dynamical properties be calculated from correlation functions that exhibit long-time constants. It is perhaps sobering to note that even a "simple" process like crystallization from a melt, close to equilibrium, is well beyond current computational tractability.

Materials design, which today is still more a process of discovery than design, is principally an investigation based upon known concepts and the acquired intuition of experimentalists. Analyzing the conditions, successful designs of new materials do not rely on a particular technique, a unique experimental observation, or an abstruse theory to be proven or disproven. On the contrary, materials design efforts critically depend upon amassing large volumes of experimentally determined data that permits an individual with deep insight to perceive an underlying pattern not previously apparent. However, given the billions of potential material systems, even with the advent of 'combinatorial chemistry', the research time and effort required to experimentally prove the existence of compounds across billions of combinations is clearly cost prohibitive.

To address this problem, the Materials and Manufacturing Directorate, together with the Air Force Office of Scientific Research (AFOSR) European Office of Aerospace Research and Development (EOARD), sponsored Dr. Pierre Villars of Switzerland to establish an international effort to address neurocomputing strategies for accelerating materials design. As a world renowned expert in crystallography and a source for many of the world's materials data handbooks, Dr. Villars' projects include such international efforts as the development of an electronic materials data base – the Linus Pauling File (LPF), a multimillion dollar program sponsored by the Japan Science and Technology Corporation Program.

The materials design project took advantage of Dr. Villars' access to quality materials data and leveraged an existing AFOSR initiative referred to as Electronic Prototyping*, involving basic research in recursive linear regression and adaptive stochastic optimization as applied to function approximation. By combining their expertise, Dr. Villars and the Electronic Prototyping research team made a significant breakthrough in April 1999 using neural networks to aid in the design of new materials. When compared to traditional (polynomial, spline or trigonometric) fixed basis expansions, neural networks utilize adaptive bases to avoid the so-called 'curse of dimensionality.' The significance is expressed as follows: whereas the approximation error for neural networks is of the order ' $1/n$ ', where n is the number of bases for traditional expansions, and the approximation error is of the order ' $1/n^{2/d}$ ', where d is the dimension of the input space (in this case the number of elemental parameters and/or expressions of them). This comparison is depicted in Figure 1.

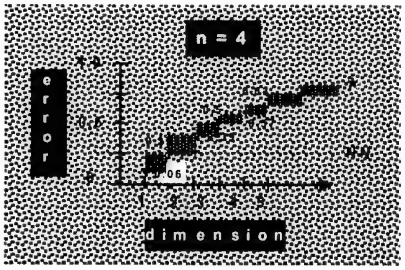

Figure 1. Polynomial, Spline, or Trigonometric Expansions

To discover or learn a relationship from experimentally determined material systems data involves one of many forms of regression, either linear, nonlinear or both. As the dataset begins to approach 1000 patterns (material systems) and/or 100 parameters (elemental properties), the complexity limits, if not precludes, any traditional expansions because predictions are critically dependent upon function approximation accuracy.

In a first step toward predicting new material systems, this effort resulted in the discovery that a nonlinear expression, involving an elemental material property, could be used to predict the occurrence of a compound for a multi-element (binary, ternary, etc.) materials system. This material property, referred to as the Mendeleev number (Figure 2), was originally conceived by D.G. Pettifor in 1984 (Oxford University, England) to group binary compounds by structure type. The use of the Mendeleev number for predicting compound formation will save time and resources relative to exploring future, yet-to-be-realized, material systems, particularly those among the four mil-

lion quaternary, or four element systems, for which little data exists.

Of the various quaternary systems of specific Air Force interest are the high temperature superconductors (e.g., Y, Ba, Cu, O), photonics/optical semiconductors (e.g., In, Ga, As, P), piezoelectrics (e.g., Pb, Zr, Ti, O), and a host of other compounds exhibiting unique combinations of properties. Furthermore, this discovery will narrow the search space of new materials and encourage the pursuit of predicting even more specific information relative to new material systems, such as stoichiometries, crystal structures, and intrinsic properties. Relative to these and other material systems, this discovery will enable a computational approach in determining which combinations of elements will yield compounds that may lead to potentially useful materials. Longer term, this ability to computationally predict compound formation will motivate the continued pursuit of computational methods to predict specific combinations of properties, which ultimately will enable an end-user to select a material or material alternatives by simply specifying operational requirements.

In addition to Dr. Villars, the research team members included: Dr. Steven LeClair and Dr. Al Jackson, Materials and Manufacturing Directorate; Professor Yoh-Han Pao (one of the world's preeminent authorities on neural networks) and Dr. Boris Igelnik, Case Western University; Professor Mark Oxley, Air Force Institute of Technology; Professor Mike Kirby, Colorado State University; Professor Bhavik Bakshi, Ohio State University; and Professor Phillip Chen, Wright State University.

* Dr. Neal Glassman of the AFOSR Math and Space Sciences Directorate manages the Electronic Prototyping Initiative.

This article was written by Dr. Steve LeClair of the Air Force Research Laboratory's Materials and Manufacturing Directorate. For more information contact TECH CONNECT at 1-800-203-6451 or visit the web site at http://www.afrl.af.mil *(Technology Transfer). Reference document ML-99-02.*

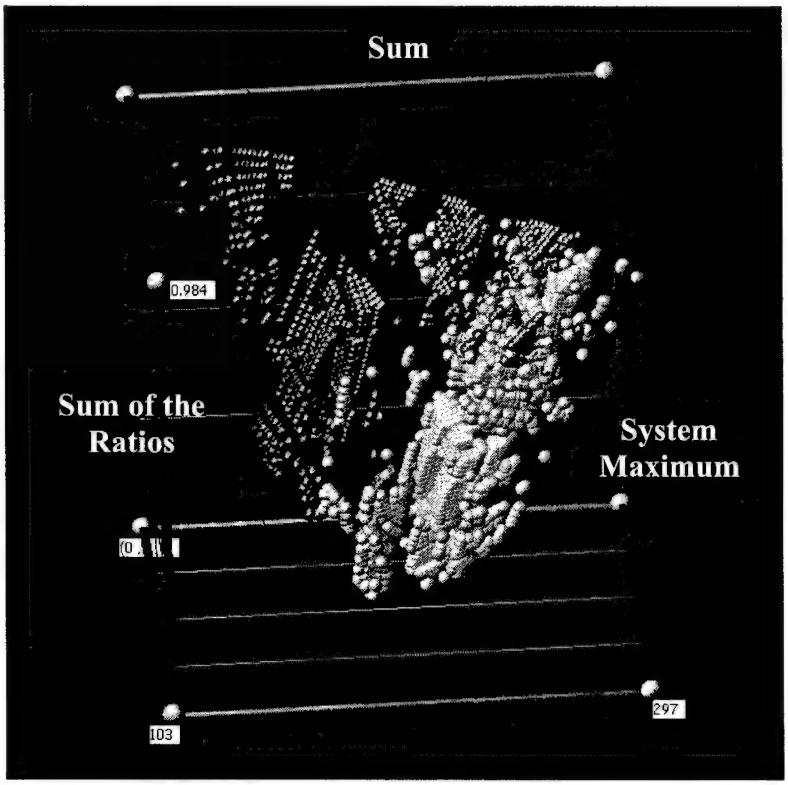

Figure 2. Three Expressions of the Mendeleev Number
(formers are Blue and nonformers are Gold)

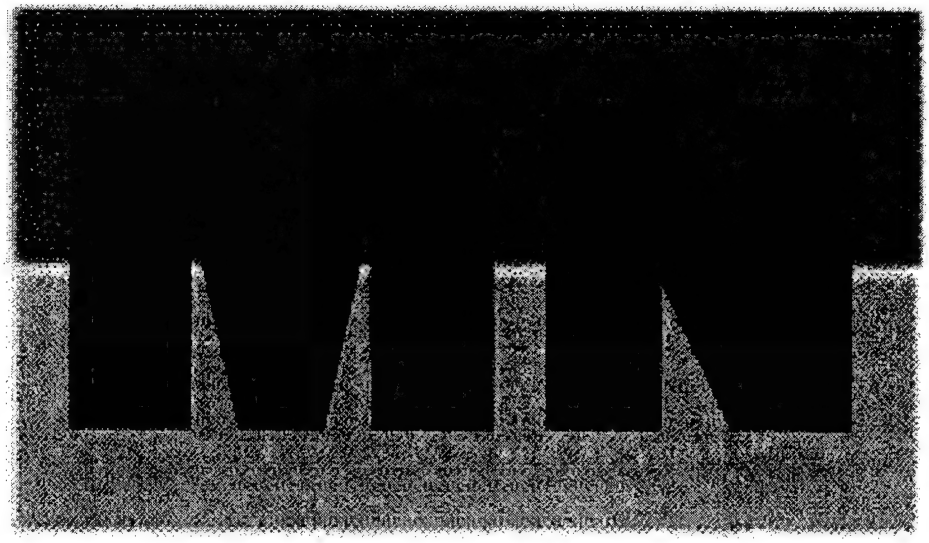

Munitions Directorate

Waterjet Technology Used in Green Munitions Program

Munitions recycling begins with waterjet technology.

AFRL's Munitions Directorate, Ordnance Division, Energetic Materials Branch, Eglin AFB, FL.

The Munitions Directorate is conducting a research and development program to recover, reuse, and/or dispose of excess, obsolete, or waste explosives and munitions systems. The objective of the green munitions program is to evaluate emerging technologies for their environmental and economic impacts on the munitions acquisition life cycle. Current projects include recovery of munitions hardware and energetic fills using high-pressure waterjet technology, reclamation of nitramines from melt/cast and plastic bonded explosives, and destruction of energetic material slurries using molten salt oxidation.

High-pressure water washout or "hydromining" is the first step in the demilitarization process. This process uses a two-stage waterjet system, see Figure 1, to separate plastic bonded explosive (PBX) fills from the warhead casings and to create a PBX/water slurry for post-process treatment. In the first stage, the explosive fill is removed in large fragments from the warhead casing using a single multi-jet nozzle with x-y-z and rotational motion. In the second (maceration) stage, these PBX fragments are reduced to particles ranging from 100 mesh to 1/8 inches (149 micron to 3.1 mm) in size by using a 6-nozzle rotating manifold in combination with a vibratory screen separator. The slurry, nominally 1/3 PBX and 2/3 water, is temporarily stored in a stirred holding tank until recycling/disposal. The process uses a closed-loop water system to recycle processed water back to a 2000 gallon holding tank that feeds the pump. Water treatment consists of a sequence of sand, 10-micron pleated paper, and activated carbon filters. The water is pumped by a 150 horsepower, horizontal triplex positive displacement pump that provides a flow rate of 14.5 gallons per minute and a nozzle pressure of up to 15,000 psi.

The warhead and waterjet assembly rest on a tilt table adjustable from 0 to 20 degrees of incline. The nozzle and stainless steel lance are supported by carbon composite sleeve to minimize deflection (0.5" maximum) of the cantilevered length. The lance has an x-y-z work envelope of 17" by 17" by 112", a 1 to 400 inch per minute (ipm) linear cut speed, and a 600 ipm rapid traverse speed. A miniaturized video camera housed in the sleeve allows observation of the hydromining operation and inspection of the interior of the warhead casing.

The hydromining operation is similar to a computer-aided machining operation in that the lance/nozzle is directed in preprogrammed movements to cut around such obstacles as interior conduits. All operations are controlled remotely via a man-machine interface screen that communicates with the local programmable logic controllers. The washout system is designed for warhead sizes ranging from 250 lbs to 2000 lbs. Inventory and developmental warheads that have been programmed include the BLU-109, MK-84, MK-82, MMT, AUP, and JAST-1000. The system has been used to remove inert fills from munitions subjected to sled-track testing and PBX fills (*e.g.*, PBXN-109) from new warheads.

This article was written by Mr. Donald Littrell of the Air Force Research Laboratory's Munitions Directorate. For more information contact TECH CONNECT at 1-800-203-6451 or visit the web site at http://www.afrl.af.mil *(Technology Transfer). Reference document MN-99-01.*

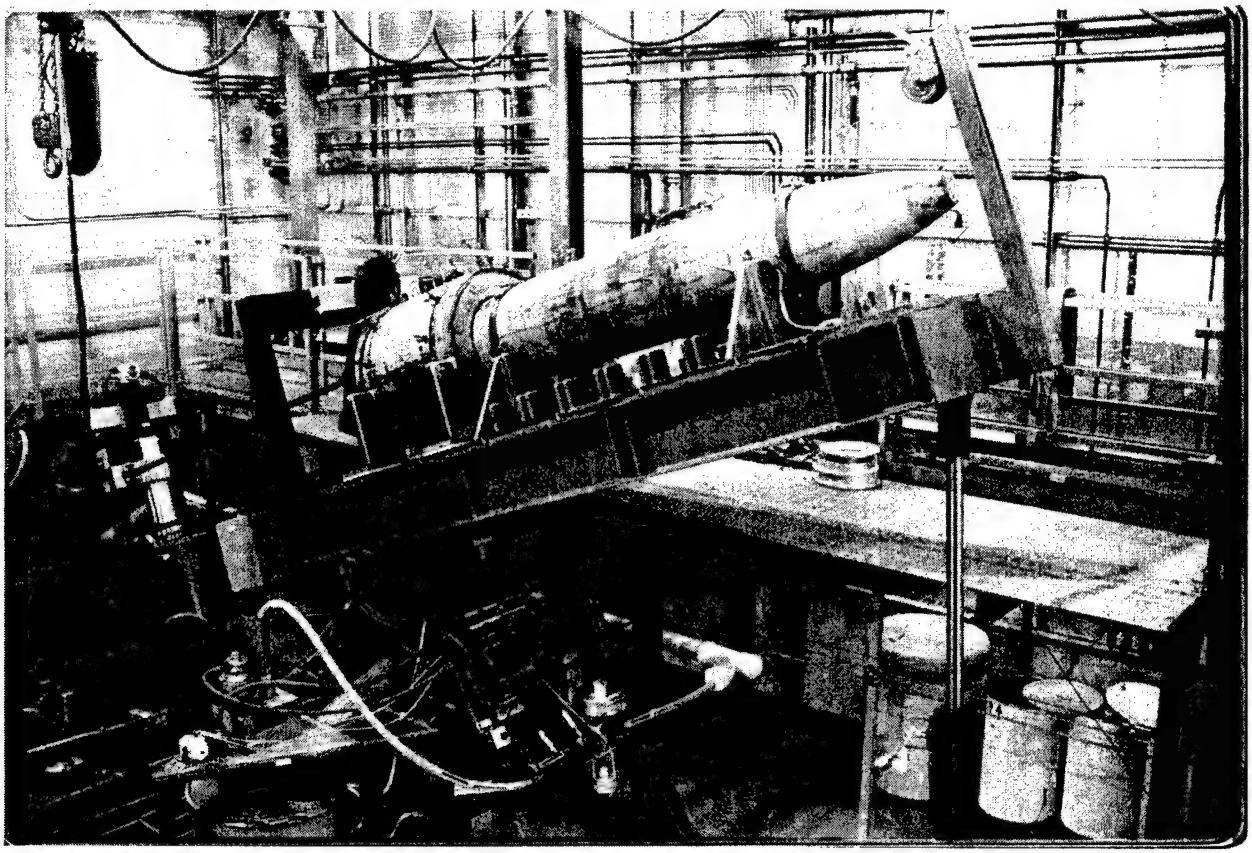

Figure 1 – Warhead washout system at the High Explosives Research and Development (HERD) facility.

Air Force Office of Scientific Research

Dip-Pen Nanolithography

Air Force to Benefit with Smaller, Lighter, Less Costly Systems.

AFRL's Air Force Office of Scientific Research, Chemistry and Life Sciences Directorate, Arlington, VA.

Microelectronics has always been limited by the size of the components that make up a device. There may no longer be a limitation with the invention of a new tool for preparing molecule-based nanostructures. "Dip Pen Nanolithography" (DPN) was recently invented by Northwestern University researchers with the support of an Air Force Office of Scientific Research (AFOSR) funding grant.

The invention of DPN, which has created the world's smallest pen, will catalyze many advances in the emerging areas of nanotechnology and molecule-based electronics. This advance will enhance the possibility of future Air Force weapon systems becoming smaller, lighter, and less expensive.

Specifically, DPN is the missing link in the nanotechnology arena that will allow development of smaller, lighter weight, faster, and more reliably produced:

- electronic circuits and devices,
- high-density storage materials, and
- sensory structures.

Use of the DPN technology could be used to create many small-scale sensors and power assemblies mounted on a single chip for use on micro-satellites or mounted within an Unmanned Aerospace Vehicle (UAV). The savings in launch weight provides for significant savings in launch costs.

This new concept in nanolithography is based upon the transport of a chemically reactive material or "ink" from the tip of a conventional silicon nitride Atomic Force Microscope (AFM) to the surface of interest or "paper." The process takes advantage of a tiny droplet of water that naturally forms between the AFM tip and surface of interest, and serves as the ink-transport medium. The chemisorption of ink to the paper is the driving force that moves the ink from the AFM tip through the water to the paper as the tip is scanned across this paper. Adjusting scan rate and relative humidity can control line widths. The relative humidity controls the size of the water droplet between the AFM tip and surface of interest and, therefore, the effective contact area between pen and paper. The current line-width resolution is 15 nm and spatial resolution is less than 10 nm. These parameters are limited by the tip radii of curvature associated with conventional AFM tips, but in principle, can be decreased through improvements in tip fabrication technology. DPN is a direct-write nanolithographic process where one can pattern and image with the same tool. These capabilities set DPN apart from almost all other nanolithographic methods and should allow one to construct "multi-ink" nanostructures and incorporate multiple chemical functionalities on a single nanochip. The method is remarkably general and easy to use, as it employs low-cost instrumentation and can be implemented under routine laboratory conditions.

This article was written by Maj Hugh C. De Long of the Air Force Research Laboratory's Air Force Office of Scientific Research. For more information contact TECH CONNECT at 1-800-203-6451 or visit the web site at http://www.afrl.af.mil (Technology Transfer). Reference document OSR-99-02.

"Perfect" Mirror Design Technology

Applications will range from communications to radiation emission control.

AFRL's Air Force Office of Scientific Research, Chemistry and Life Sciences Directorate, Arlington, VA.

A significant discovery in mirror design technology, which began with Air Force Office of Scientific Research (AFOSR) funding, offers potential for vast improvements in many Air Force applications. Massachusetts Institute of Technology (MIT) researchers and graduate students have invented a "perfect" mirror which combines the best features of the two previously known types of mirrors, metallic and dielectric, by reflecting light at any angle with virtually no energy loss. Among other benefits, the anticipated advance will provide:

- large diameter, low-loss mirrors in space for advanced communication and surveillance systems,
- coatings on aerospace systems with controlled radiation emission in specific frequency ranges, and
- advanced optical and optoelectronic systems such as non-mechanical laser beam steering devices.

The discovery of the new mirror technology resulted from a design innovation created by MIT professor, Edwin L. Thomas, and graduate student, Yoel Fink, in collaboration with other researchers from MIT's Department of Materials Science and Engineering, Department of Physics, and the Plasma Science Fusion Center. The MIT team expanded the existing layering design concepts used to create mirrors. Their "perfect" mirror permits truly omnidirectional reflectivity. The design is sufficiently generic so that it can be used to cover many different radiation frequency ranges of interest, offering immense potential for military and commercial applications.

Metallic and dielectric mirrors each have their limitations. Metallic mirrors, the most common type like those on medicine cabinets, waste energy by absorbing a small fraction of the light that falls on them.

Dielectric mirrors, unlike metals, are not conductive and therefore reflect light more efficiently. Light travels in dielectric materials at speeds that are lower than in air. When light traveling in a particular direction through one type of dielectric material encounters another type, part of the light is reflected while the other part is transmitted at a different angle.

Conventional dielectric mirrors are made of multiple layers of transparent dielectric materials. Such materials, which can be made to be extremely low-loss compared to their metallic counterparts, are used to reflect a prescribed range of frequencies coming from within a limited set of angles. Such dielectric mirrors are used in devices such as lasers, which need very high reflectivity.

The new type of dielectric mirror developed at MIT can reflect light from all angles and polarizations, just like metallic mirrors, but also can be as low-loss as dielectric mirrors. In addition, it can be "tuned" to reflect certain wavelength ranges and transmit the rest of the spectrum. A device such as this, operating in the visible light, would appear to be one color, red for instance, while also being transparent.

The researchers demonstrated the new design by fabricating a mirror comprised of nine alternating layers of polystyrene (a plastic) and tellurium. The mirrors are made using polymer processing techniques that allow the manufacture of very high-quality optical devices for relatively low cost with minimal specialized equipment. In addition, the materials are relatively common, easy to process, and can be used for applications covering large areas.

Because of the ease in processing, this type of mirror can be coated on to practically any surface. This opens doors for many imaginative applications and devices. For example, "omniguides" comprised of rolled, spaghetti-thin tubes of the new "perfect" mirror material can be fabricated to guide light over a very long distance without loss. By minimizing the energy absorption characteristics, the need for amplifiers is reduced. Additionally, the new technique allows mirror design to be optimized as a planar film for specific reflective ranges and can serve as an efficient heat radiator or collector. Coated walls, windows, or even car interiors could very efficiently reflect heat while maintaining transparency. Applications for cellular telephones, photovoltaic batteries, and lightweight insulator clothing are also anticipated. Figure 1 is an artistic rendition depicting a 20-meter diameter telescope, known as Gossamer Proteus (a Directed Energy Directorate concept), which uses a near net-shape film. This reduces weight and complexity of the satellite system. The AFOSR funded MIT research may provide a space-deployable, low-loss reflective surface for this type of application.

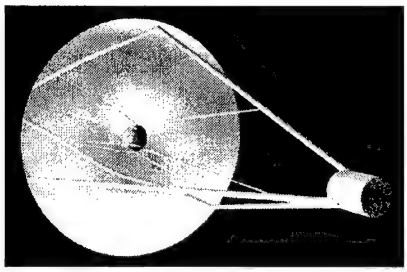

Figure 1. Optical Telescope Satellite in Space

This article was written by Dr. Charles Lee of the Air Force Office of Scientific Research. For more information contact TECH CONNECT at 1-800-203-6451 or visit the web site at http://www.afrl.af.mil (Technology Transfer). Reference document OSR-99-04.

"Stress Check" for Composite Bonded Aircraft Structures

Composite Structure Designers Benefit From New Analysis Tools

AFRL's Air Force Office of Scientific Research, Mathematics and Space Sciences Directorate, Arlington, VA.

Aerospace materials scientists and structural engineers now have a new state-of-the-art software product called *Stress Check™*, which provides efficient and reliable analysis tools for composite bonded aircraft structures. A composites research team from the aeronautics industry, known as the Composites Affordability Initiative (CAI), has just completed an extensive study of current capabilities in the area of failure analysis tools for composite bonded joints. This study led the CAI team to unanimously choose *Stress Check* as the software tool to replace, as well as radically improve, existing industry standard software currently used for sizing bonded joints.

This new software tool will play an important role in making composites more affordable for the next generation fighter aircraft. The software provides a highly reliable and user-friendly production stress analysis tool that will replace the Finite Element Method (FEM) tools and failure criteria experts currently employ for analyzing bonded joints. The software includes a FEM-based handbook format that allows non-experts to utilize models prepared by specialists. The handbook models include built-in failure criteria, geometric and material nonlinearities, and the modern FEM technology that provides better error control and treatment of very large aspect ratios.

This software is based on Air Force Office of Scientific Research (AFOSR)-sponsored research on new failure methodologies for composite materials and modern finite element technology pioneered by Prof. Barna Szabo at Washington University in St. Louis. His work led to the development of the modern p-version of the finite element method with a *posteriori* error control, new hierarchical modeling techniques in elasticity and composite materials, and new failure initiation criteria.

Stress Check, developed through a collaboration between Washington University scientists and Engineering Software Research and Development, Inc. (ESRD) in St. Louis, was partially sponsored by an AFOSR Phase II small business technology transfer (STTR) contract. The CAI team in conjunction with ESRD, recommended modifications to *Stress Check* ensuring its reliability, portability, and ease of use. ESRD is currently implementing these improvements through AFOSR sponsorship. Once the modifications are in place, the CAI endorsement will result in the use of *Stress Check* for bonded joint analysis throughout the aeronautics industry. The CAI team has involved extensive DoD and industry participation. Representation has included the Air Force Research Laboratory; the Naval Air Systems Command; Lockheed Martin companies in Fort Worth and Marietta; Boeing companies in Seattle, St. Louis, and Long Beach; Northrop Grumman companies in Bethpage NY and El Segundo CA; and General Electric Aircraft Engines in Cincinnati.

This article was written by Dr. Marc Jacobs of the Air Force Research Laboratory's Air Force Office of Scientific Research. For more information contact TECH CONNECT at 1-800-203-6451 or visit the web site at http://www.afrl.af.mil (Technology Transfer). Reference document OSR-99-03.

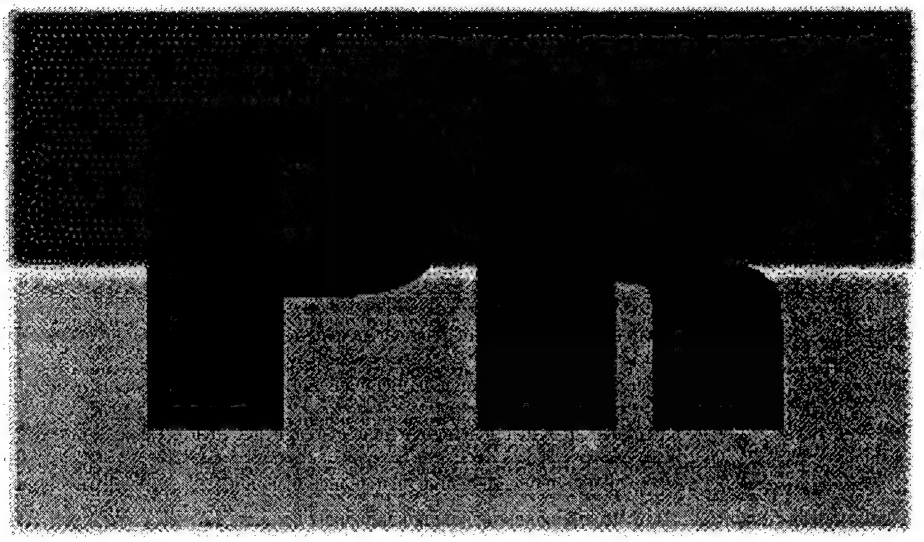

Propulsion Directorate

Additive Improves Performance of Heating/Cooling Systems

Military technology transfer helps keep the public comfortable at home, at work, or in the car.

AFRL's Propulsion Directorate, Power Division, Power Generation and Thermal Management Branch, Wright-Patterson AFB, OH.

A unique patented refrigerant additive called QwikBoost™ has been developed that can improve the performance of air conditioners, heat pumps, refrigerators, and freezers. QwikBoost™ is already impacting the automotive air conditioning market, and can significantly impact the appliance/home air conditioning and heat pump market due to its tremendous potential to reduce energy costs.

QwikBoost™ is the product of an Air Force Phase II Small Business Innovation Research (SBIR) program with Mainstream Engineering Corporation of Rockledge, FL. The Air Force originally embarked on the program with Mainstream Engineering as part of a Civil Engineering Research program to reduce the energy consumption of Air Force heating/cooling systems. The Air Combat Command (ACC) can use the technology represented by QwikBoost™ for its mobile airbase thrust, which endeavors to locate an airbase anywhere in the world. The energy savings achieved by improved heating/cooling system performance will significantly enhance ACC's capability.

The recent phase-out of the chlorofluorocarbon (CFC) refrigerants that dominated the market for many years motivated QwikBoost's™ development. In the 1970's, researchers presented a theory that CFCs posed a threat to the Earth's ozone layer. In the mid-1980's, measurements indicated depleted ozone layers over Antarctica. Experts blamed CFCs for the depleted ozone layer and took action to prevent further damage. In 1987, 24 nations and the European Economic Community signed the Montreal Protocol to limit the production of CFCs, and the U.S. implemented this agreement through the Clean Air Act. This law called for the complete phase-out of production and importation of CFCs by January 1, 1996. Since then, the only useable CFCs are those obtained from recovery, recycling, and reclamation. This regulation signaled the end for CFCs, and a new class of refrigerants, hydrofluorocarbons (HFCs), replaced CFCs. HFCs pose no risk to the ozone layer, however, the performance of HFC refrigerants falls short of their CFC predecessors.

The Clean Air Act significantly impacted the automotive industry. Automobile manufacturers discarded air conditioning systems using CFC refrigerants (R-12) in favor of systems utilizing HFC refrigerants (R-134a). Also, due to the diminishing supply of CFCs, many older cars were retrofitted with air conditioners that operate on R-134a. Owners of cars with air conditioning systems using R-134a refrigerant, however, suffered from decreased cooling performance.

QwikBoost™ is an absorbent fluid additive that has a high affinity for HFC and HCFC refrigerants. This affinity is due to the fact that the additive hydrogen bonds to refrigerants containing hydrogen. This hydrogen bonding results in a lowering of the vapor pressure of the refrigerant and also results in a heat of solution when the absorbent and refrigerant are mixed. The additive is nontoxic, nonflammable, and nonvolatile. Its freezing point is well below the normal freezer operating range. It has zero ozone depletion potential. Materials compatibility tests have shown it to be noncorrosive to metals and compatible with common elastomer materials.

Based on the success achieved in the AFRL program and the needs of the automotive industry, Mainstream Engineering decided to market a commercial refrigerant additive for automotive air conditioning systems. This additive, QwikBoost™, is the solution for under-performing R-134a-equipped automobile air conditioners. QwikBoost™ improves cooling performance by effectively increasing the refrigerant's latent heat of vaporization; the energy required to change the refrigerant from a liquid to a gas. Demonstrations of QwikBoost™ in R-134a automotive systems and refrigerator/freezer systems show marked performance and cooling capacity improvements. For automotive air conditioners, increased cooling capacity translates to more rapid cooling of the car's interior and greater passenger comfort. This enhanced performance is especially desirable for automobile air conditioning systems retrofitted with R-134a refrigerant, since the original system design calls for the better performing R-12 refrigerant.

QwikBoost™ is now on the consumer market for automotive air conditioners. It comes in a handy 3-ounce R-134a-pressurized can that allows easy introduction into automotive air conditioning systems (see Figure 1). Addition of QwikBoost™ to the air conditioning system occurs in the same simple fashion as charging the system with refrigerant. In fact, QwikBoost™ addition uses the same charging hose used for refrigerant additions (see Figure 2). One application of QwikBoost™ to the cooling sys-

tem lasts for the active life of the system and never requires replacement. QwikBoost™ became commercially available for automotive air conditioners in 1998. It should debut in home appliances by the year 2000 and in residential air conditioners by 2003. The projected savings to the nation's energy costs amounts to billions of dollars per year, thus, the ultimate winner is the public.

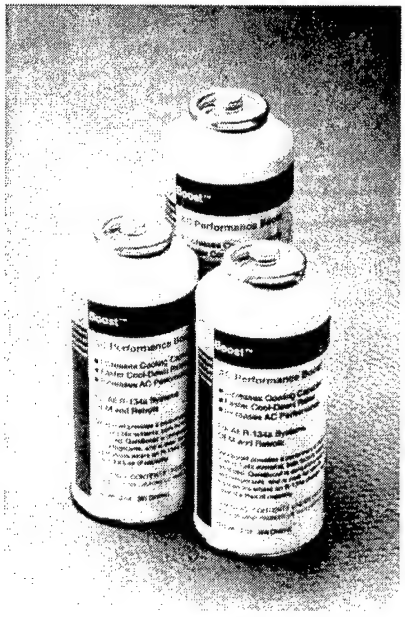

Figure 1. Cans of QwikBoost™ automotive refrigerant additive

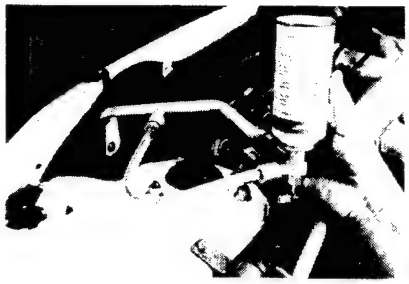

Figure 2. QwikBoost™ being added to an automotive air conditioning system

Though QwikBoost™ provides a significant improvement to cooling performance (see Figure 3), it is also important to note the compatibility with components of the cooling system. Lubrication and compressor life tests performed with QwikBoost™ indicate no adverse effects on system lubrication or compressor life. Lubrication tests performed by an independent laboratory show that QwikBoost™ actually improves wear properties compared to the lubricant alone. Over 100,000 hours of compressor life tests performed on reciprocating, scroll, and rotary compressors also gave excellent results. These tests indicate QwikBoost™ reduces accumulation of wear metals in the lubricant. Thus, it appears QwikBoost™ not only improves cooling system performance, but also may reduce system wear and extend system life.

Because of QwikBoost's™ energy and environmental benefits, those associated with its development received recognition for their achievements. Mainstream Engineering garnered the prestigious Tibbett's Award at the White House in 1997. Furthermore, the Federal Laboratory Consortium recently awarded Joseph M. Gottschlich, the Air Force Program Manager for the "Hybrid Cycle Heat Pump" program that led to the development of QwikBoost™, the Federal Laboratory Consortium Award for Technology Transfer.

This article was written by Joseph M. Gottschlich and Jeffrey A. Pearce (contractor) of the Air Force Research Laboratory's Propulsion Directorate. For more information contact TECH CONNECT at 1-800-203-6451 or visit the web site at http://www.afrl.af.mil (Technology Transfer). Reference document PR-99-06.

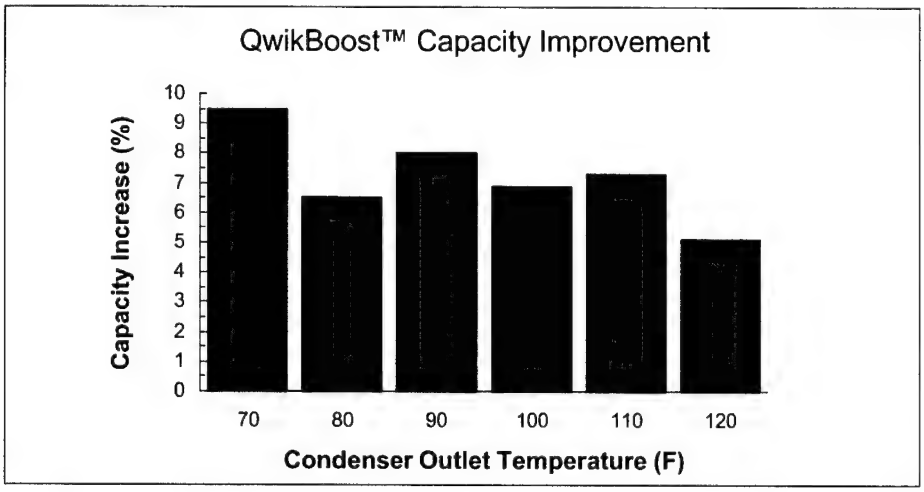

Figure 3. Improvement in cooling capacity using QwikBoost™

Sensors Directorate

Higher Operating Temperatures for Ultra-High-Density Optical Memories Based on Spectral Hole Burning

Raman-excited spin coherence is used to increase the operating temperature of spectral hole burning optical memories while maintaining storage density.

AFRL's Sensor Directorate, Electromagnetics Technology Division, Optoelectric Technology Branch, Hanscom AFB, MA.

As the amount of data generated by future Air Force sensors increases, the need for fast storage and processing becomes more urgent. Optical memories based on spectral hole burning have the ability to meet these future needs because of their potential for extremely high-density storage. This high-density storage is possible because these memories store many bits of data (up to 10^5) at each spatial location. This is accomplished by using an inhomogeneously broadened optical transition so the maximum number of bits stored at each location is given by the ratio of inhomogeneous to homogeneous line-widths. To achieve a very narrow optical homogeneous width, and therefore a high storage density, it is necessary to eliminate broadening caused by phonons by cooling the memory to a temperature near that of liquid helium. This requirement has so far limited the widespread application of spectral hole burning memories because of the complexity and costs associated with the necessary cryogenics.

This work explores the use of Raman-excited spin coherence to increase the operating temperature of spectral hole burning memories. The approach is based on the observation that spin coherence, especially for nuclear spins, is much less strongly coupled to the environment than optical coherence. In fact, the first experiment to demonstrate the concept of spectral hole burning memories was performed at room temperature using spin echoes. Since this demonstration was performed with microwave excitation, the storage density was limited by the large microwave wavelength. This limitation can be overcome by using spin coherence excited by Raman-resonant laser beams.

To demonstrate optical data storage using Raman-excited spin coherence, a crystal of Pr^{3+} doped Y_2SiO_5 (Pr:YSO) was used. Figure 1 shows an energy level diagram of Pr:YSO at site 1 on the $^3H_4 \leftrightarrow {}^1D_2$ transition, which has a resonant frequency of 606 nm. The optical homogeneous width is about 3 kHz and the inhomogeneous width is ~ 4 GHz. The ground state population decay time T_1 is ~100 s, and spin transverse decay time T_2 for the 10.2 MHz transition is 500 s at 6 K, and its inhomogeneous line-width is 29 kHz.

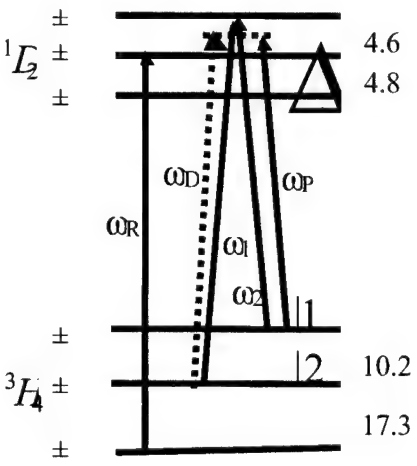

Figure 1. Schematic energy level diagram of Pr:YSO site 1.

To store data, a spin coherence is created between the ground states $|1\rangle \leftrightarrow |2\rangle$ (shown in Figure 1) by the two resonant optical write beams ω_1 and ω_2. To measure this ground state coherence, a probe beam ω_P is red-detuned by Δ = 1.5 MHz from the frequency of the beam ω_2. This probe (read) beam scatters off on a spin coherence grating created by the write beams and generates the four-wave mixing signal ω_D, satisfying the phase matching condition $\mathbf{k_D=k_1-k_2+k_P}$. A re-pump beam ω_R is used to prevent depopulation of states $|1\rangle$ and $|2\rangle$ due to spectral hole burning.

Figure 2 shows a schematic of the experimental setup. Acousto-optic modulators (AOM) driven by frequency synthesizers generate the four required laser beams ω_1, ω_2, ω_R, and ω_P from the dye laser output. All laser beams are forward propagating, circularly polarized with a quarter wave plate, and focused into the sample (Pr:YSO) by a 40cm focal length lens. The size of the crystal is 3×6×9 (mm) with its symmetric optical B-axis along the 9 mm direction. Driving each AOM with the output of a digital pulse generator (DG1, DG2, etc.) via a power amplifier (PA) creates pulses. The laser beams are focused onto the sample with a lens (L) and a beamsplitter (BS) is used to deflect the diffracted beam onto a photodiode (PD). The signal is averaged by a boxcar averager (BOX) and viewed on an oscilloscope (O) and chart recorder (CR). The light transmitted by BS is viewed on a screen (SC) giving the spot pattern shown in Figure 2.

Figure 3 demonstrates optical data storage using Raman-excited spin coherence. The schematic pulse sequence is shown at the top of the figure. Each input pulse is composed of both resonant Raman beams ω_1 and ω_2.

Figure 4 shows the spin T_2 versus temperature. Each spin T_2 is measured from the 'two-pulse' echo intensity (see echo pulse e in Figure 3) versus the write pulse delay with pulses d' and r absent. The write pulse delay time was varied from 100 μs to 900 μs. Within the measurement fluctuations, the spin T_2 appears constant up to 6 K. Beyond 6 K, the signal was too weak to make accurate measurements even though echoes were detected as long as there was spectral hole burning (up to ~ 8 K).

To compare the spin coherence temperature dependence to that of the optical coherence, the optical coherence time T_2 is estimated by measuring the intensity of the 'two-pulse' echo at a fixed write pulse delay (see Figure 5). The echo intensity should be proportional to the square of the optical T_2. As seen in Figure 5, the echo intensity decreases exponentially above 4 °K. This implies the optical T_2 and, hence, the storage capacity expected for non-Raman optical hole burning also decrease exponentially as temperature goes up.

The observed temperature independence of the spin coherence lifetime, while the optical coherence lifetime rapidly shortens, demonstrates the potential of Raman-excited spin coherence to increase the operating temperature of spectral hole burning memories.

Although the improvement in operating temperature achieved in this proof-of-principle experiment is modest, it opens the door to greater future improvements as better Raman-echo storage materials are identified. With each factor of 2 to 3 increase in operating temperature, the necessary cryogenic technology becomes significantly cheaper and the number of applications to take advantage of the tremendous potential of spectral hole burning rapidly increases.

This work was performed by Dr. Philip Hemmer of the Air Force Research Laboratory's Optoelectric Technology Branch of the Sensors Directorate. For more information contact TECH CONNECT at 1-800-203-6451 or visit the web site at http://www.afrl.af.mil *(Technology Transfer). Reference document SN-99-06.*

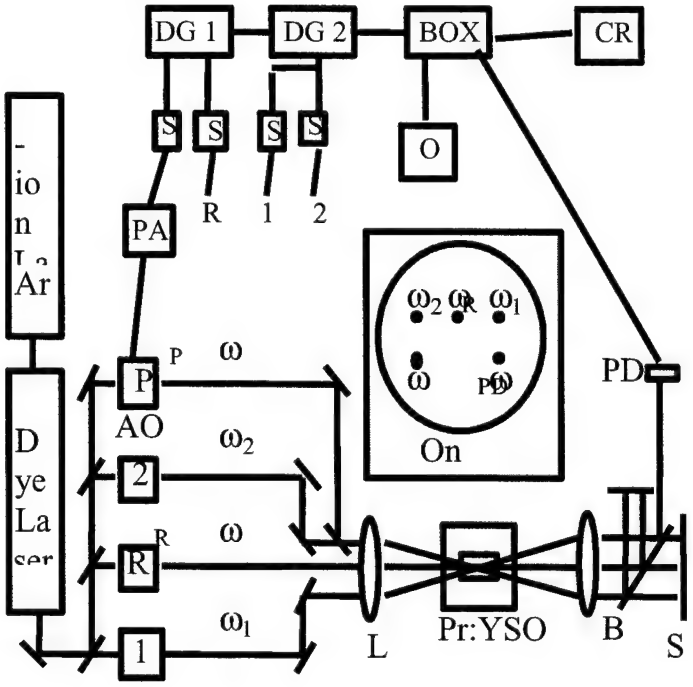

Figure 2. Schematic of experimental setup for exciting transient spin coherences (echoes).

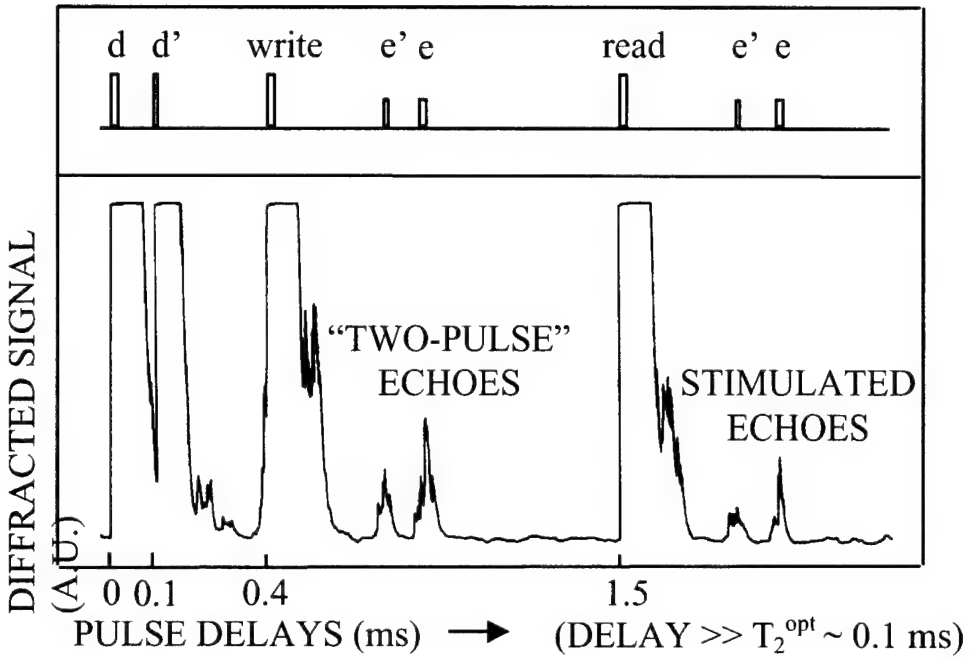

Figure 3. Demonstration of optical data storage using Raman-excited spin coherence.

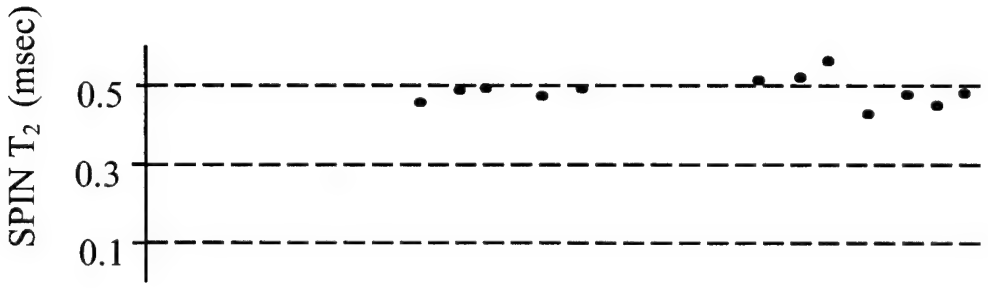

Figure 4. Experimentally measured Raman spin coherence lifetime as a function of temperature.

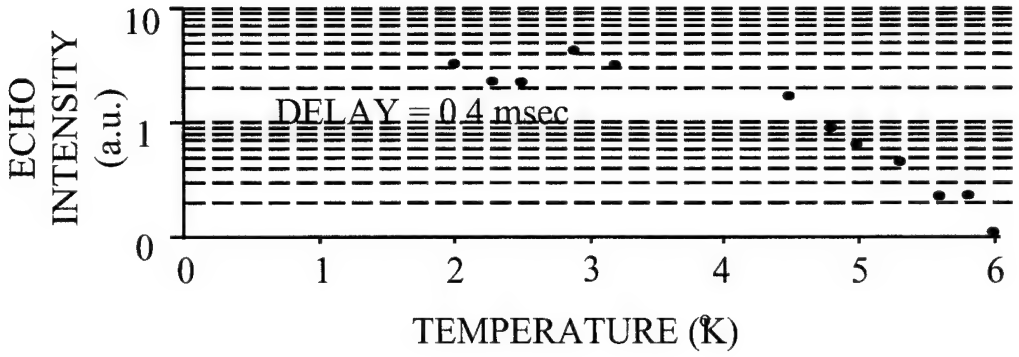

Figure 5. Raman echo intensity as a function of temperature.

Optical Limiting in Hydrothermal Zinc Oxide Crystals

Two-photon absorption and a negative nonlinear refractive index make Zinc Oxide (ZnO) an effective optical limiter, with potential applications for sensor protection and laser stabilization.

AFRL's Sensors Directorate, Electromagnetics Technology Division, Electromagnetic Materials Branch, Hanscom AFB, MA.

Wide band-gap semiconductors have attracted substantial interest for applications in solid-state electronics and optics. The basic promise of wide band-gap materials in electronics is that of enabling high temperature devices and high power devices. High temperature operation is a result of the exponential decrease of the concentration of intrinsic carriers with increase in band-gap at any given temperature. Intrinsic carrier concentrations of order $10^{15}cm^{-3}$ occur at 300 °C for Silicon (Si), 500 °C for Gallium Arsenide (GaAs) and over 1000 °C for wide band-gap semiconductors such as Gallium Nitride (GaN) and ZnO.[1] High power operation is a result of one order of higher magnitude breakdown fields, for the wide band-gap semiconductors, compared to Si or GaAs. In optics, wide band-gap semiconductors are attractive for the development of blue and ultraviolet light emitting diodes and lasers.

ZnO is a II-VI semiconductor with a wide band-gap of 3.37 eV, a direct gap band structure[2] at room temperature, and an exciton binding energy of 60 meV.[3] The combination of high excitonic and biexcitonic oscillator strength and good high temperature characteristics make ZnO a promising material for optical applications. It has been used as a visible and ultraviolet photoconductor and as fluorescent material. Its piezoelectric and acusto-optic properties have also been exploited in the past.[4] Interest in ZnO has intensified as a result of its crystallographic properties that could make it a suitable substrate for wide band-gap nitride semiconductor devices,[5] and possibly for ultraviolet/blue/green lasers and detectors as well. Both GaN and ZnO have a Wurtzite crystal structure, similar bandgaps, and closely matched lattice parameters.[6] This article reports nonlinear optical properties of ZnO that make it an attractive candidate for optical limiting applications.

Researchers at the Sensors Directorate grew ZnO crystals in platinum-lined, high-strength steel hydrothermal autoclaves. Sealed platinum liners were employed to isolate the crystal growth environment from the walls of the autoclave, which otherwise would have reacted chemically with the high-pH mineralizing solution.[7] The mineralizing solution was a mixture of Li_2CO_3, 4 N KOH, and 4 N NaOH, with a fill quantity of 80%. The nutrient was prepared from 99.99% pure ZnO powder (Alfa Aesar, particle size less than 3 μm). The powder was sintered in a platinum crucible for four hours at a temperature of 1350°C. The seeds used were [0001] plates of ZnO obtained from previous hydrothermal growth runs. During growth, the nutrient zone was held at 355°C, with a temperature gradient of 10°C declining towards the seed zone. Growth rates in the [0001] direction on the basal seed plates averaged 10 mm per day for the 30-day runs.

Wafers were sliced and the C+ and C- planes identified by etching in nitric acid following the method developed by Mariano and Hanneman.[8] Surface properties were analyzed by double axis x-ray rocking curve. Room temperature photoluminescence and low temperature photoluminescence measurements were also obtained and the results have been reported elsewhere.[9] For crystal growth in the [0001], or C+ direction, the growth rate was faster and the crystal was clear to light yellow in color. For the [000$^-$1], or C- direction, the growth rate was one-third as fast and the color was clear with a light green hue. Speculation is that the differences in color are due to an imbalance in incorporation of unintentional impurities between the C+ and C- sectors. The green (C-) sector contains about twice as much iron impurity as the yellow (C+) sector. The C+ sector has twice as much aluminum and Si as the C- sector. They also have different resistivity and free carrier concentrations.[8] Another possible explanation is that stoichiometric defects, combined with impurities, may act as compensation centers in the C+ sector, giving rise to a reduced free carrier optical absorption.

The picosecond pulses used in the experiments were obtained from a Quantel model YG 501c Neodymium-doped Yttrium Aluminum Garnet (Nd:YAG) laser. It comprises oscillator and amplifier stages. The amplified fundamental beam is passed through a second harmonic generator crystal to obtain approximately 30 mJ per pulse of 532 nm radiation. The output pulse width is 30 picoseconds. The laser is operated at a repetition rate of 6.7 Hz.

The Z-scan technique,[10] a single beam technique that allows the determination of the sign of the nonlinear index of refraction and the nonlinear absorptive behavior, was employed. The normalized transmittance for measurements taken in the far field through a small aperture, plotted

against the sample position, exhibits a valley-peak trace for the positive nonlinear refractive index as the sample is translated across the focal plane from - z to + z, and a peak-valley trace for a negative nonlinear refractive index. When no aperture is present and all the light transmitted through the sample is collected, the traces represent changes in absorption. Saturable absorption yields a peak centered at z = 0, and reverse saturable absorption yields a valley.

For samples with sizeable refractive and absorptive nonlinearities, closed aperture Z-scan measurements contain contributions from both the intensity-dependent changes in the transmission and the intensity-dependent changes in the refractive index. Dividing the normalized closed aperture Z-scan data by the normalized open aperture Z-scan data can retrieve the phase distortion produced by the change in the index of refraction.

The Z-scan measurements obtained for the ZnO crystals exhibit a negative nonlinear index of refraction and two-photon absorption. Open aperture and the ratio of closed-to-open aperture Z-scan results are shown in Figures 1 and 2 for one sample. By numerically fitting the power limiting data, researchers obtained 2 cm/GW for the two-photon absorption coefficient β and -1×10^{-5} cm^2/GW for the nonlinear index of refraction n_2.

Optical power limiting traces, shown in Figure 3, were obtained by placing the ZnO sample at the focal plane in the Z-scan setup and varying the input light intensity. No damage was observed for the ZnO crystal cut from the C+ sector at intensities of order 70 GW/cm^2.

An interesting application of optical power limiters is the stabilization of the output of a laser whose pulses have a large degree of fluctuation from shot to shot. To check the suitability of the ZnO crystals for shot-to-shot stabilization, histograms of the laser power energy fluctuations without and with a ZnO crystal in front of it were recorded. The output of the laser was tightly focused just before the front face of the crystal in order to maximize the combination of two-photon absorption and negative nonlinear index of refraction. The results, shown in Figures 4a and 4b, demonstrate significant laser stabilization when ZnO is employed as a power limiter.

Contributing authors in this research include Meckie T. Harris, Michael J. Callahan, John S. Bailey, Michael J. Suscavage, and David F. Bliss of the Sensors Directorate. The Air Force Office of Scientific Research (AFOSR) supported this work, in part. Francisco J. Aranda is grateful to the National Research Council for financial support.

References

[1] S. C. Binari and H. B. Dietrich, "III-V Nitride Electronic Devices," in *Optoelectronic Properties of Semiconductors and Superlattices: Vol. 2. GaN and Related Materials*, M.O. Manashreh, series ed., and Stephen J. Pearton, ed., Gordon and Breach Publishers, Amsterdam, The Netherlands (1997), p. 513 ff.

[2] Y. Ohta, T. Haga, and Y. Abe,"Crystallographic features of ZnO single crystals," Jpn. J. Appl. Phys., **36** (1997) L1040.

[3] D. M. Bagnall, Y. F. Chen, Z. Zhu, and T. Yao, "High temperature excitonic stimulated emission from ZnO epitaxial layers," Appl. Phys. Lett., **73** (1998) 1038.

[4] T. Shiosaki, N. Kitamura, and A. Kawabata, Proc. IEEE Ultrasonics Symp. (1991) p. 296 ff.

[5] B. N. Sverdlov, G. A. Martin, H. Morkoc and D. J. Smith, "Formation of threading defects in GaN wurtzite films grown on nonisomorphic substrates," Appl. Phys. Lett. **67** (1995) 2063.

[6] D. C. Reynolds, D. C. Look and B. Jogai, "Optically pumped ultraviolet lasing from ZnO," Solid State Comm. **99** (1996) 873

[7] R. R. Monchamp, "Growth of Zinc Oxide Crystals-Interim Engineering Progress Report," Airtron Division of Litton Industries, Morris Plains , New Jersey, ASD Project Nr.7-988, Contract No. AF33(657)-8795, November 1964.

[8] A. N. Mariano and R. E. Hanneman, J. Appl. Phys. **34** (1963) 384.

[9] M. J. Suscavage, M. T. Harris, D. F. Bliss, P. Yip, S. Q. Wang, D. Schwall, L. Bouthillette, M. J. Callahan, J. S. Bailey, D. C. Look, D. C. Reynolds, R. L. Jones and C. W. Litton, "High quality hydrothermal ZnO crystals," MRS Internet J. Nitride Semicond. Res. **4S1,** G3.40 (1999).

[10] M. Sheik-Bahae, A. A. Said, T. Wei, D .J. Hagan, E. W. Van Stryland, "Sensitive measurement of optical nonlinearities using a single beam," IEEE J. Quant. Elect. **46**, (1990) 760.

This article was written by Francisco J. Aranda of the Air Force Research Laboratory's Sensors Directorate. For more information contact TECH CONNECT at 1-800-203-6451 or visit the web site at http://www.afrl.af.mil *(Technology Transfer). Reference document SN-99-12.*

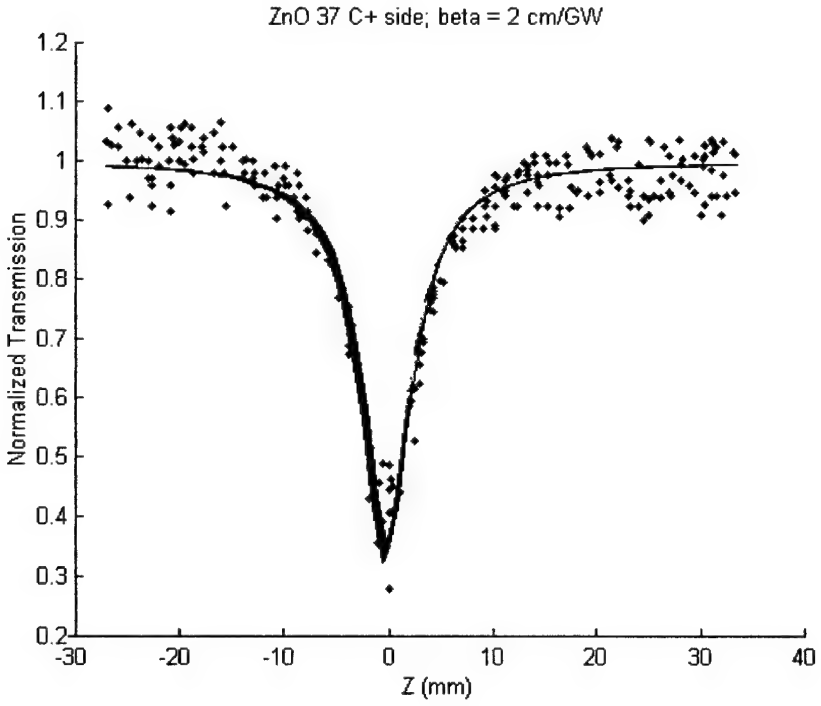

Figure 1. Open aperture Z-scan result.

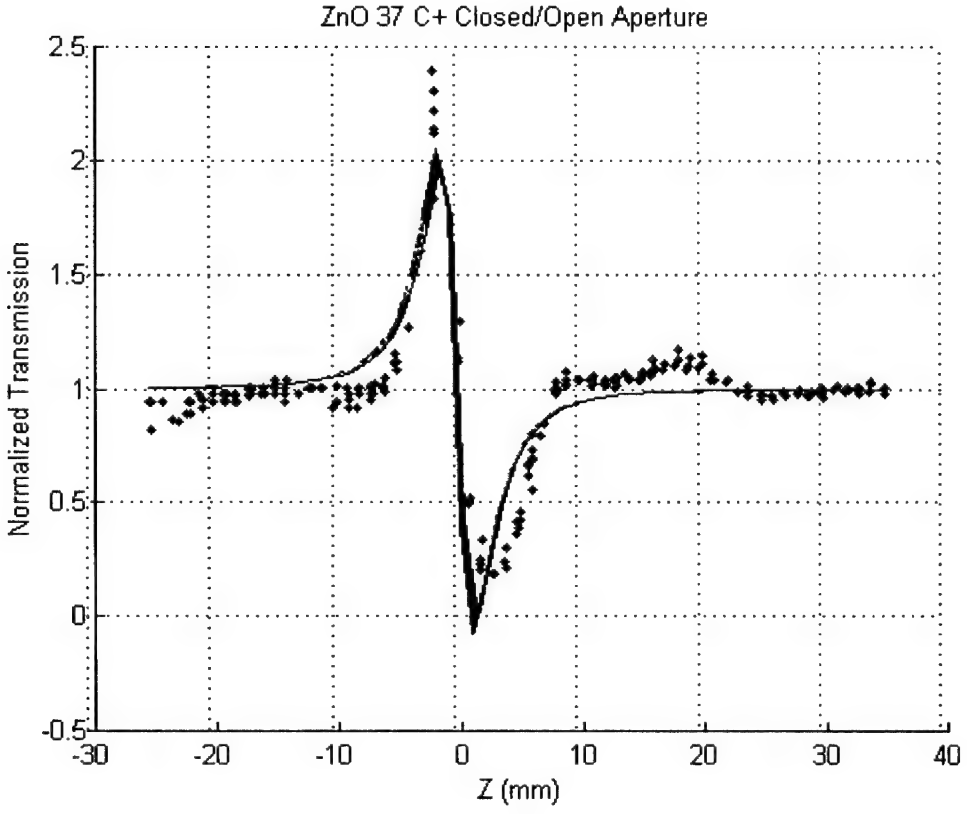

Figure 2. Result of the division of closed and open aperture Z-scans.

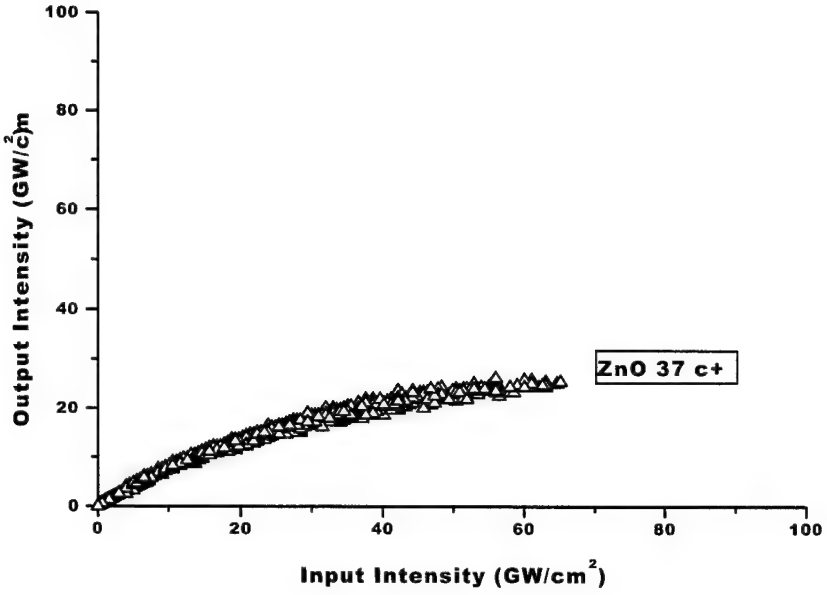

Figure 3. Optical Power Limiting Curve for a 1.63 mm thick ZnO crystal cut from the C+ sector.

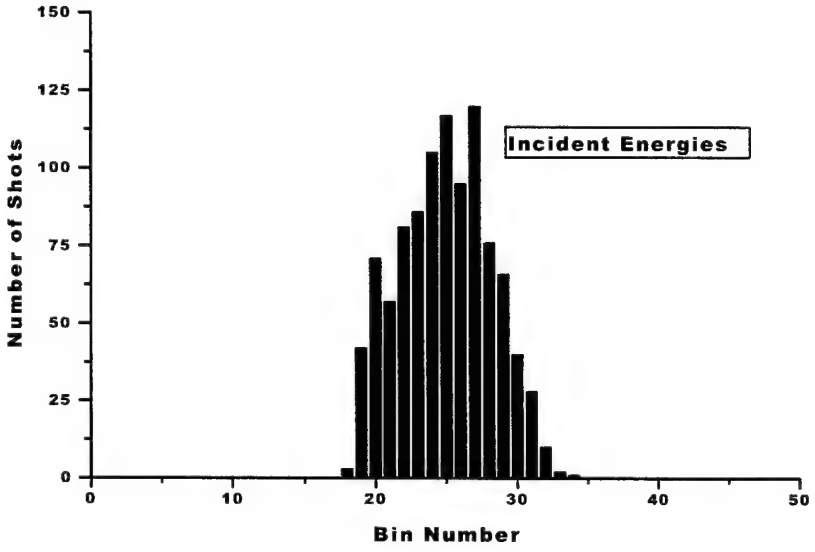

Figure 4a. Histogram of the distribution of the laser pulse energy for 1000 shots.

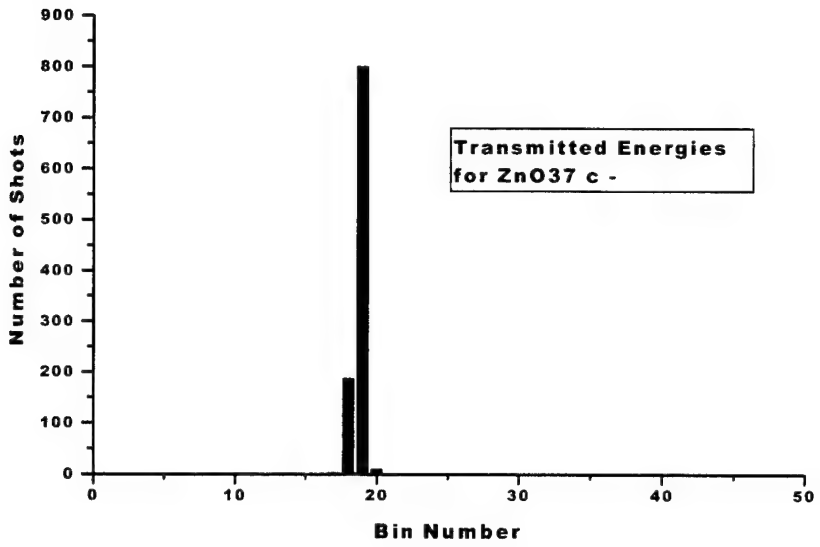

Figure 4b. Histogram of the distribution of the transmitted pulse energy for the same 1000 shots

Air Vehicle Directorate

38 Active Core Exhaust Control

Active Core Exhaust Control

Pulsed air injection systems for high-bypass ratio turbine engines to enhance plume mixing.

AFRL's Air Vehicles Directorate, Aeronautical Sciences Division, Integration and Demonstration Branch, Wright Patterson AFB, OH.

Active Core Exhaust (ACE) control is a fully integrated, non-intrusive pulsed injection system which destabilizes the core-exhaust plume resulting in enhanced mixing of the plume and the surrounding air. The destabilized, flapping of the plume is induced by injecting a small amount (1.5%) of high-pressure compressor bleed air perpendicular to the core exhaust flow at the core nozzle exit. As seen in Figure 1, the enhanced mixing results in a significant and rapid decrease of the exhaust plume temperature.

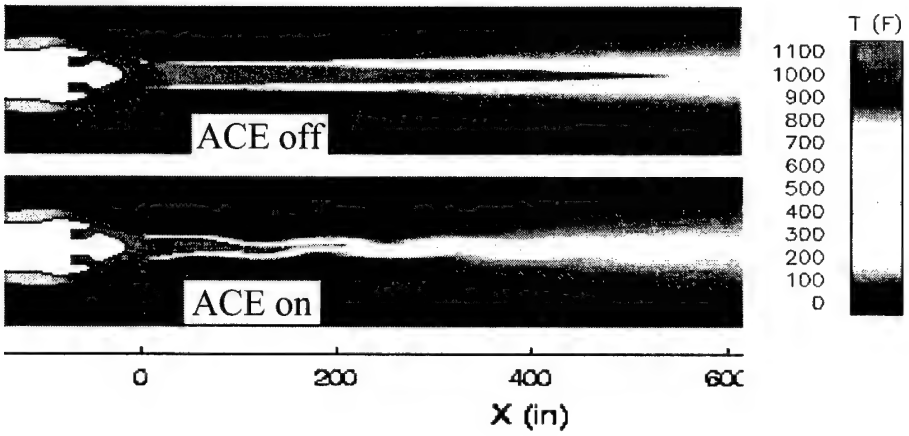

Figure 1. Effect of ACE Control on Plume Temperature

The reduced exhaust temperature permits removal of the Core Thrust Reverser (CTR) on the C-17 aircraft. Analysis and data indicate the CTR is not required to meet the C-17's backing requirements and is primarily used to maintain Human Effectiveness temperature requirements for the load masters during engine-running ground operations.

ACE is an on-demand system, meaning that it can be turned off and on, depending upon the flight conditions and mission scenario. Since ACE is an on-demand system, it can be used to reduce the thermal load on the trailing edge flaps during take-off and descent and then turned off during the cruise phase of the mission. Also, since ACE allows deletion of the CTR, the thermal load on the leading edge slats encountered during backing operations is also eliminated, thus, permitting the use of high temperature aluminum in place of titanium.

Integration of the ACE control system will reduce the cost of each new C-17 aircraft built by approximately $1.2M and reduce the weight of every C-17 aircraft built or retrofitted by approximately 1200 lbs.

By incorporating ACE and deleting the CTR, a derivative benefit is obtained by allowing the integration of a plug nozzle as shown in Figure 2. The plug nozzle provides 90% - 95% line-of-sight blockage to the hot engine components during all phases of the mission.

This program addresses the Air Mobility Command's need to reduce cost and weight of the C-17 transport aircraft, while enhancing its survivability. It also addresses the Air Logistic Center's desire to enhance aircraft supportability and maintainability. Application of this technology addresses these needs as follows:

1) elimination of maintenance on the core thrust reverser,
2) retention of working environment temperature levels at the rear of the aircraft during engine-running ground operations required to meet Human Effectiveness standards,
3) reduction of thermal loading on trailing edge flaps during powered lift operations,
4) reduction of thermal loading on leading edge slats during backing operations, and
5) enhancement of survivability by integration of a plug nozzle.

The technical approach used to implement the ACE control technology requires a redesign of the core nozzle and deletion of the core thrust reverser. The redesigned nozzle will fully integrate all tubing and injector channels into the shell of the nozzle and the current engine housing. The redesign does not change the external profile of the nozzle. The compressor bleed air will be extracted from an existing port at the 17th stage and routed through a fluidic actuator, which diverts the bleed air to the appropriate injector. This actuator, which does not have any moving parts, is designed to provide a constant load to the compressor bleed port, therefore, the engine does not sense the pulsing of the injectors.

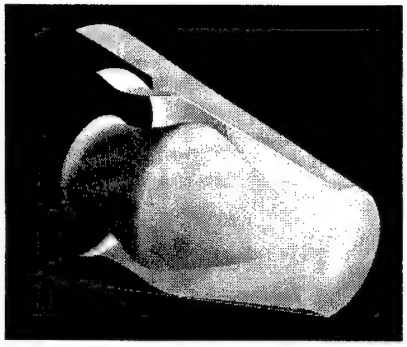

Figure 2. Redesigned Plug Nozzle

A significant amount of research and risk reduction has already been performed on this project. A proof-of-concept ground test with the low-bypass ratio JT8D engine was performed in 1997. This test demonstrated the engine continues to operate normally when ACE is turned on. A 50% reduction in exhaust plume temperature 10 nozzle diameters downstream of the exit is a realistic expectation. This test also allowed variation of many injection variables including, but not limited to, injection pulse frequency, mass flow rate, injector orientation and injector size.

The ground test with the low-bypass ratio engine also provided experimental data which has been used to develop and validate a Computational Fluid Dynamics (CFD) model for use in trade studies of the high-bypass ratio design.

In a concurrent effort to redesign the nozzle and optimize injection parameters, a trade study evaluating six flight conditions was performed. Based on the analysis of take-off, cruise, penetration, maximum reverse, idle reverse, and airdrop scenarios, a reasonably mature configuration for the nozzle and the ACE control system was established, as illustrated in Figure 3.

Testing of the new configuration will occur in early CY00 at the Pratt-Whitney test facility used for the low-bypass ratio engine test.

This article was written by Captain Clarence Chenault of the Air Force Research Laboratory's Air Vehicles Directorate. For more information contact TECH CONNECT at 800-203-6451 or visit the web site at http://www.afrl.af.mil *(Technology Transfer). Reference document VA-99-05.*

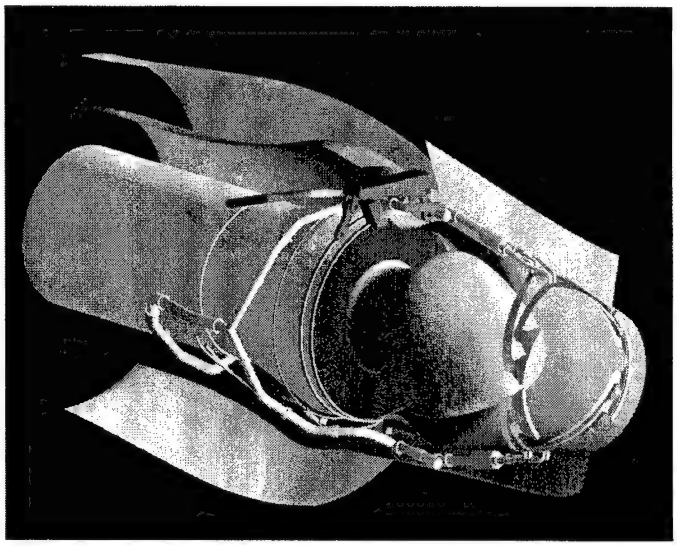

Figure 3 - Integrated ACE Control System and Plug Nozzle

First Flight Test Demonstration of Neural Network Software

The RESTORE Reconfigurable Control for Tailless Fighter Aircraft X-36 Flight Test Program successfully demonstrated a damage/fault tolerant neural network adaptive flight control system on a tailless unmanned air vehicle.

AFRL's Air Vehicles Directorate, Aeronautical Sciences Division, Flight Dynamics and Control Branch, Wright-Patterson AFB, OH.

A RESTORE team, comprised of Boeing, NASA Dryden, NASA Ames, and AFRL, successfully flew the neural network adaptation algorithm on the X-36 tailless fighter aircraft. The neural network was integrated into the existing X-36 flight control system, demonstrating the retrofit capability of this technology. Piloted hardware-in-the-loop-simulation (HILS) testing helped mature the reconfigurable control laws and evaluate their robustness for a variety of simulated actuator failures. During the X-36 flight tests, a wing trailing-edge control surface failure was simulated. The RESTORE neural network successfully adapted the control law to account for the failure, thus validating the HILS results.

The original X-36 program was led by NASA's Ames Research Center and was funded under a roughly 50/50 cost sharing arrangement with Boeing. NASA Ames was responsible for continued development of critical technologies, while Boeing was responsible for design, fabrication and flight testing. The X-36, shown in Figure 1, demonstrated that tailless aircraft can exceed the agility levels of present day fighters. NASA Dryden Flight Research Center's experience on the Highly Maneuverable Aircraft Technology (HiMAT) program with Ames led to the decision to avoid installing redundant flight control systems. The result was that the cost of the X-36 was approximately one-fourth that of the HiMAT in comparable year dollars.

RESTORE is an Air Force Research Laboratory advanced development program, whose purpose is to develop reconfigurable flight control algorithms. Unlike traditional reconfiguration methods, RESTORE control laws compensate for unknown aircraft damage as well as actuator failures by continuously adapting to the changing dynamic behavior of the aircraft. Two contract awards were made in 1996, one to Lockheed Martin Tactical Aircraft Systems and the other to Boeing Phantom Works. Both contractors developed unique approaches to address the following areas: on-line control design, on-line system identification, on-line control allocation, and command limiting. These algorithms were systematically integrated into tailless fighter aircraft models (which are aerodynamically unstable in multiple axes), thus enabling predictable handling qualities for the pilot. The algorithms were also developed within a modular architecture to provide a way of seamlessly inserting control technology advances and transitioning the technology to other aircraft.

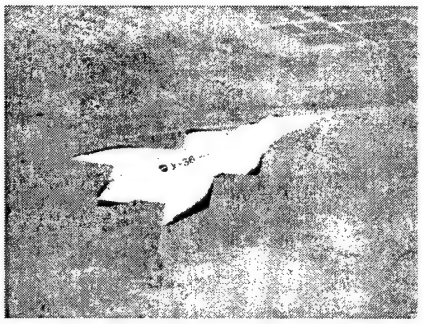

Figure 1. The X-36 demonstrates the maneuver capability of a tailless fighter and is dynamically unstable in the longitudinal and directional axes.

The Boeing RESTORE team based their design on a modular control architecture with dynamic inversion (Figure 2). Dynamic inversion utilizes an on-board model of the aircraft dynamics to cancel the actual aerodynamics; it then adds the desired dynamics to achieve good handling qualities. The neural network was developed to adaptively regulate the inversion error between the embedded aircraft model and the true aerodynamics. Such an inversion error can occur because of model uncertainty, actuator failure, or aircraft damage. A second module, the control allocation, is used to distribute the desired control response from the control algorithms to the control actuators. Depending on aircraft response, the control allocation algorithms prioritize critical axes while optimizing for particular mission objectives, such as stealth or maneuver load alleviation. A third RESTORE module, system identification, uses a least squares algorithm to estimate aerodynamic parameters. Null space injection is used to briefly excite control surfaces to obtain these estimates without significant performance degradation.

AFRL and NAVAIR jointly sponsored the RESTORE X-36 flight tests to demonstrate a portion of the RESTORE technology on existing, flight-proven control laws. The X-36 vehicle provided an excellent demonstration platform because it was a twenty eight percent scale model of a tailless fighter aircraft with a flight control system also based on dynamic inversion. This aircraft provides redundant, multi-axis conventional control surfaces, split flaps, and

yaw thrust vectoring for maneuvering, thus providing reconfiguration capability for simulated control surface failures.

The neural network was integrated into the existing X-36 flight control system, demonstrating the retrofit capability of the RESTORE technology. HILS testing was used to mature the reconfigurable control laws and evaluate their robustness for a variety of simulated actuator failures. The control laws were given no prior knowledge of the simulated failure input. While performing the HILS testing, the RESTORE control laws were frequently compared to the baseline flight control laws. The RESTORE algorithms demonstrated departure resistance to aggressive failures and enabled acceptable handling qualities, as shown in Figure 3. Flight tests at NASA Dryden verified the HILS results, as a wing trailing-edge control surface failure was simulated in flight, and the RESTORE neural network adapted the control law to account for the failure.

In addition to the limited flight testing completed in December 1998, the full RESTORE technology was demonstrated using high fidelity aircraft piloted simulations in the summer of 1999. The Self-Adaptive Flight Experiment (SAFE), planned to begin in 2001, will flight demonstrate the complete RESTORE control technology package on a hypersonic demonstration platform. Finally, Boeing has adopted the RESTORE control architecture as the baseline flight control system for the DARPA/AFRL Boeing Unmanned Combat Air Vehicle (UCAV) program, which is scheduled for flight demonstration in 2001.

RESTORE control laws provide cost-efficient architectures designed to update the control laws in real-time on-board the aircraft, in addition to providing tolerance to actuator failures and battle damage. The RESTORE modular control-law architecture will reduce development costs and encourage technology insertion. It is possible to retrofit this technology into existing flight control systems, as demonstrated by the successful X-36 flight tests. Another advantage of this emerging technology is that it is readily transferable to other digital flight control air vehicles, including those in the private sector. RESTORE flight control algorithms will significantly improve commercial aviation safety by providing on-board reconfiguration capabilities.

This article was written by Lt. Eric B. Nelson of the Air Force Research Laboratory's Air Vehicles Directorate. For more information contact TECH CONNECT at 1-800-203-6451 or visit the web site at http://www.afrl.af.mil *(Technology Transfer). Reference document VA-99-04.*

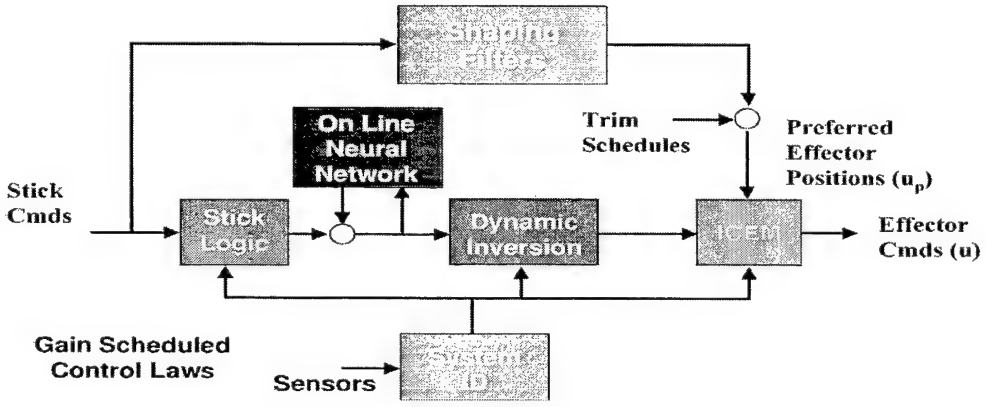

Figure 2. Boeing's RESTORE technology is based on dynamic inversion and minimizes dependence on system identification. This modular structure is particularly conducive for technology transfer to other flight control systems using dynamic inversion, including that found on the X-36.

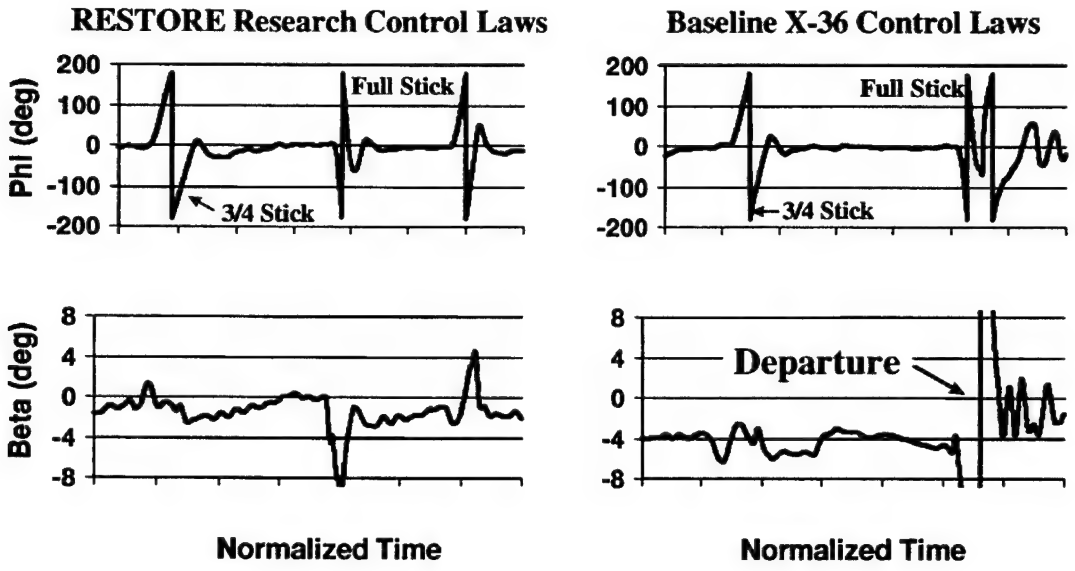

Figure 3. RESTORE technology enhances departure resistance during aggressive maneuvers under failure. The X-36 is performing a 360-degree Roll during HILS testing, with left split flaps locked at 100% maximum deflection.

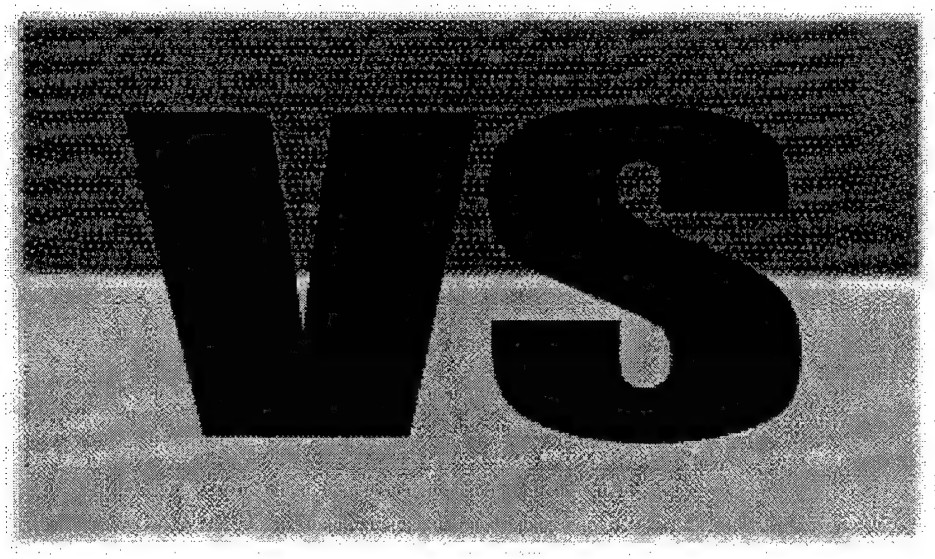

Space Vehicles Directorate

Treacherous High Ground: The Near Earth Space Environment

Air Force investments to study space environmental effects are of strategic national interest.

AFRL's Space Vehicles Directorate, Battlespace Environment Division, Space Physics Models Branch, Hanscom AFB, MA.

Since its inception, the U. S. space program has been integrally related to our strategic national defense, providing a practical implementation of Eisenhower's "Open Skies" proposal to minimize the risk of an accidental outbreak of general warfare. Space-related treaties negotiated by the Kennedy, Johnson, Nixon, and Carter administrations assured the integrity of our national technical means of verification. During the Gulf War, U.S. space intelligence assets allowed the undetected flanking maneuver that abruptly ended the conflict. In light of the U.S. national treaty obligations, "space control" has special significance in improving technologies that enhance the national defense operational capabilities in space and ensuring that systems perform reliably. However, critical spacecraft components degrade and die or they can fail catastrophically from interactions with hazardous environments or from hostile human forces. In the foreseeable future, natural processes pose significantly greater dangers to the reliable operation of our space assets than enemy action. For this reason, Air Force investments to understand dangers to satellites in the near Earth space environment and develop measures to mitigate their worst effects are in the strategic national interest.

Air Force satellites orbit planet Earth which is approximately 150 M km (8 light minutes) from the sun, commonly regarded as a uniformly luminous body that remains unchanged from day to day. Galileo's sunspots are often easily dismissed as inconsequential surface blemishes; however, at least two misperceptions need to be addressed. First, while the sun appears placid at visible wavelength that originates in the photosphere, emissions from the corona are quite dynamic at ultraviolet and x-ray wavelengths. Figure 1 shows two simultaneous images from the Japanese satellite, Yohkoh. The image on the left was taken at visible wavelengths, while the image on the right results from iron (Fe) emissions at x-ray wavelengths. A sequence of such images reveals constant variability in ultraviolet and x-ray emissions from the sun. Second, the solar luminosity of 4 $x10^{26}$ J/s means the sun emits the equivalent of 40 trillion megaton bombs every second with about 10^{17} J/s, (10,000 megatons per second) striking the Earth. Even small changes in total solar electromagnetic or corpuscular emissions are considered big by human standards and, in considering the U.S. strategic national interests in space, must be regarded as such.

Of particular concern are geomagnetic storms, which first manifest themselves as large, episodic variations in the Earth's magnetic field. Early satellites revealed that the Earth's magnetic field is confined by a solar wind that carries a weak magnetic flux. The most dangerous storms occur when large amounts of plasma and magnetic fields are violently ejected outward from the solar corona toward the Earth. These are called coronal mass ejections (CMEs). The energy impacting the Earth's magnetic field can reach approximately 10^{14} J/s. Ten megatons/second seems small in comparison with the normal solar flux; however, the photons (light) interact only with the Earth's atmosphere and surface. The charged particles and magnetic fields of a CME act directly on the Earth's magnetic field and the plasma it contains. The four sequential images in Figure 2 were acquired by the Solar and Heliospheric Observatory (SOHO) satellite and show the birth and initial expansion of a CME that caused a magnetic storm on Earth.

After a CME makes contact with the Earth's magnetic field, the initial effect is a contraction of the Earth's field. To achieve pressure balance with the new interplanetary environment, a large amplitude hydromagnetic wave is

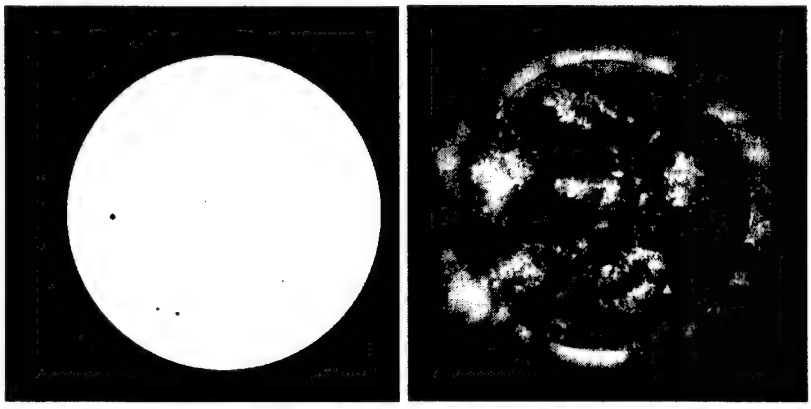

Figure 1. Image on the left taken at visible wavelengths from the Yohkoh satellite. Image on the right taken from Fe emissions at x-ray wavelengths.

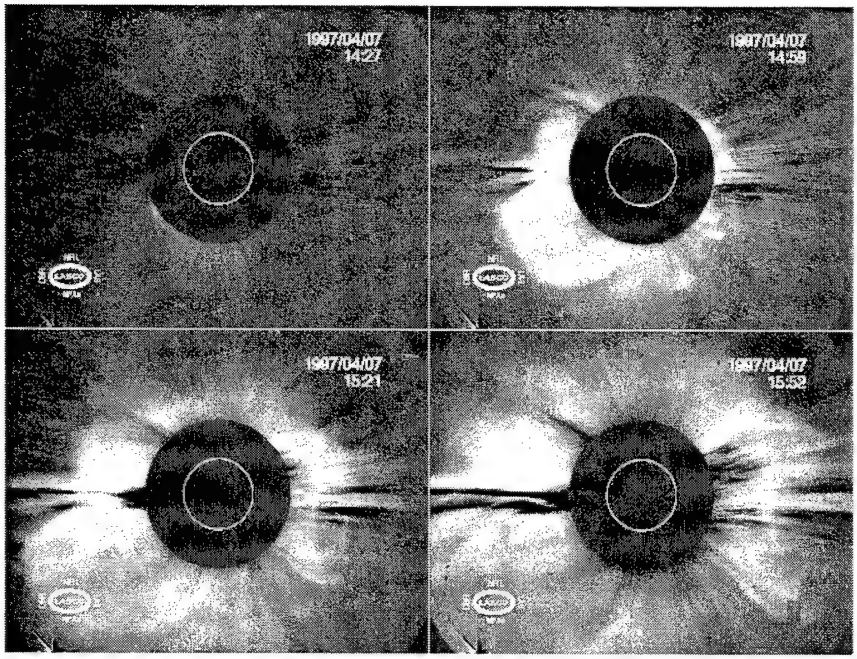

Figure 2. Birth through expansion of a CME that caused a magnetic storm on Earth, as acquired by the SOHO satellite.

launched inward. The wave's energy is partitioned between compressional and transverse magnetohydrodynamic (MHD) waves. Until March 24, 1991, the assumption was made that the compressional wave simply traveled toward the Earth and produced positive magnetic spikes called sudden storm commencements. Measurements from AFRL's Combined Release and Radiation Effects Satellite (CRRES) changed that idea. As an electromagnetic pulse passed, CRRES was instantly bathed in multi-MeV electrons and ions. Figure 3 displays the flux (number per cm^2 per second) of 10.7 MeV protons showing a new radiation belt that is formed in minutes, not days, as normally occurs. When CRRES died six months later due to a battery failure, the new radiation belt still existed. Diffuse populations of high-energy ions and electrons in the outer magnetosphere were caught up by the compressional wave and entered the inner magnetosphere, gaining energy along the way.

Microprocessors onboard satellites control the flow of information between the sensors and spacecraft components. These processors, smaller than a penny, communicate with memory cells to direct all satellite functions. On the ground and in quiet space environments, processors and memory chips are usually highly reliable. In the radiation belts, however, ionization trails, created as corpuscular radiation passes through a memory chip, can cause a malfunction. Electrical charges can accumulate in wire insulation, then migrate into computer components as currents discharge. Operating for extended periods in intense radiation environments can cause chips to decay from the effects of accumulated radiation doses.

The transverse MHD waves launched by CME impacts carry magnetically field-aligned currents that couple the ionosphere to the energized interplanetary medium. Associated electric fields cause the ionospheric plasma to circulate in two large convection cells. Looking down from above the North Pole, there is a clockwise rotating cell in the afternoon/evening sector and a counterclockwise rotating cell in the morning sector. Satellite-borne sensors have measured total potential drops of >200 kV and field-aligned currents of approximately 10 MA, coupling the magnetosphere to the high-latitude ionosphere. Three things happen immediately. First, the high latitude ionosphere brightens with auroral light, obscuring our ability to monitor strategic missile attack corridors on the Continental United States (CONUS). Second, the neutral atmosphere above 90 km heats up at a rate of 2×10^{12} J/s, or 12 megatons/minute. During the March 1989 magnetic storm, Joule heating of the upper atmosphere caused the temporary loss of approximately 3000 space catalog objects. Third, electric fields permeate the magnetosphere energizing local ions and electrons. As a storm progresses, bright auroral forms appear at much lower latitudes than normal. The optical clutter in the night sky increases immensely and the mid-latitude ionosphere becomes turbulent, disrupting long-distance communications in regions where they are normally quite stable. Energized electrons and ions migrate earthward to replenish the inner and outer radiation belts. Satellites at geostationary altitude charge to several tens of kilovolts.

In the early stages of storms, electric fields at mid- to low-latitudes drive turbulence in the nightside ionosphere, degrading the propagation of communications and navigation signals. Ionospheric turbulence significantly degraded both functions during the Gulf War and directly led to development of the Communications/Navigation Outage Forecast System (C/NOFS) satellite, which is scheduled for launch in 2003. Space Vehicles Directorate scientists are working diligently to develop the tools needed to predict ionospheric disturbances and assist the Air Force in avoiding potentially harmful disruptions of service.

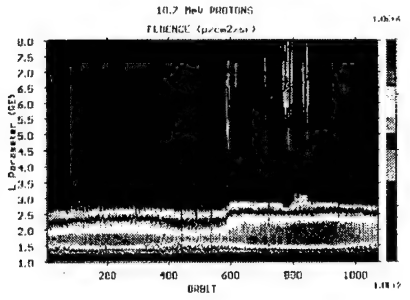

Figure 3. The flux of protons with energies of 10.7 MeV measured by CRRES. The vertical axis represents distance from the center of the earth measured in earth radii and referenced to the magnetic equatorial plane. CRRES orbit numbers on the horizontal axis represent the entire satellite's lifetime of one and a quarter years.

Since a solar maximum phase currently exists, the severe impact of solar storms may sound grim, however, the solar-terrestrial physics community is learning to exploit new technologies to mitigate the effects of storm-time disturbances.

The first step is to ensure satellite operators have adequate warning of major storms. In January 1997, both the SOHO and Yohkoh satellites observed the birth of a CME and optically tracked it to the Earth. The Advanced Composition Explorer (ACE) satellite, orbiting about a million miles above the Earth, regularly monitors the solar wind density and speed, and the interplanetary magnetic field. From these interplanetary measurements forecasters can predict the degree of magnetospheric compression and the electric potential imposed on the magnetosphere-ionosphere system approximately 45 minute ahead of time. This information is integrated with measurements from the Defense Meteorological Satellite Program (DMSP) and Television Infrared Observation Satellites (TIROS) to exercise the Magnetospheric Specification and Forecast Model and the Ionospheric Specification Model. Warnings are then issued to systems operators alerting them about the impending development of severe satellite charging environments and the possible loss of transionospheric communications links.

A second practical step is to raise situational awareness so operators know the radiation levels in which satellites are operating. Figure 4 shows a Compact Environment Anomaly Sensor (CEASE), developed by the Space Vehicles Directorate. With 1 kg of mass and 2 watts of power, CEASE monitors the energetic particle environments in which host satellites are flying. When anomalies occur, engineers can quickly determine what really happened and take appropriate corrective measures. Satellites flying at geostationary altitudes should carry small plasma thrusters that activate automatically to discharge the spacecraft, as onboard computers recognize the spacecraft is in a charging environment.

A third practical step is to develop technologies to clear the radiation belts of energetic particles within a day of a magnetic storm. This would greatly reduce dose rates to microelectronic components and prolong their operational lifetimes. Two important points must be recognized. First, the radiation belts are not dangerous because they contain many trapped energetic particles. Their total of approximately 10^{19} particles is roughly the number of molecules in a thimble of air. Rather, danger comes from the fact that they are so energetic that they can penetrate shielding to disrupt electronic components. If the average energy of the particles is 6 MeV, the total energy in the radiation belts would be about the same as a 1 ton bomb. Second, the radiation belts are cleared of energetic particles with no outside assistance within a few weeks of a storm. Naturally occurring, low-frequency radio waves interact strongly with trapped electrons and protons, which slowly migrate out of the radiation belts to orbits that penetrate the upper atmosphere.

The U.S. space assets are extremely vulnerable when exposed to these violent storms. During the past decade, microelectronics have been introduced into the space environment, but their long-range survivability in major solar storms is still unknown. New techniques have been developed to study the sun, the source of space weather. Through analyses of measurements and simulations of the coupled magnetosphere-ionosphere system, scientists can learn much more about local responses and their impact on space systems.

Storm warnings reduce risk because they allow time to implement plans to mitigate catastrophic circumstances. Satellite survivability improves when controllers can power down instruments or take active measures to discharge spacecraft as they enter hazardous environments. Viewed from this perspective, investment in forecasting space weather is in the highest national interest.

This article was written by Dr. William J. Burke of the Air Force Research Laboratory's Space Vehicles Directorate. For more information contact TECH CONNECT at

1-800-203-6451 or visit the web site at http://www.afrl.af.mil *(Technology Transfer). Reference document VS-99-04.*

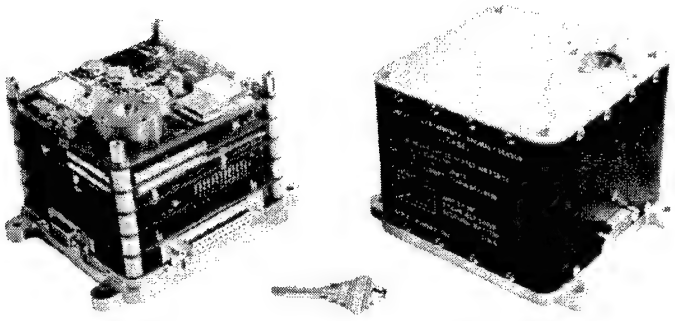

Figure 4. Compact Environment Anomaly Sensor (CEASE).

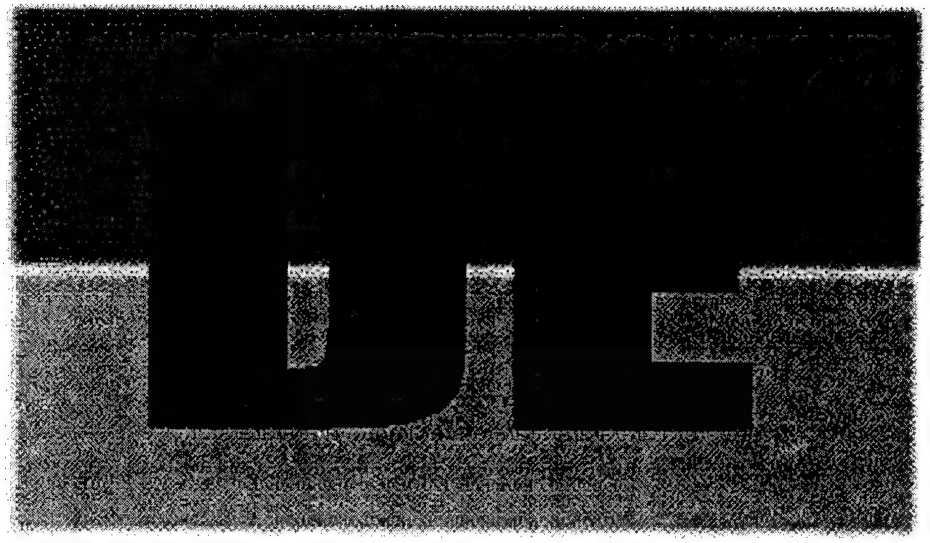

Directed Energy Directorate

Biophotonics Applications of High-Power Semiconductor Diode Laser Technology

Dual-use medical applications of high-power diode lasers and solid-state lasers are critically important due to the enormous potential for portability, compactness and their effective interaction with tissue.

AFRL's Directed Energy Directorate, Laser Division, Cooperative Development Branch, Kirtland AFB, NM.

The Directed Energy Directorate (DE) is contributing greatly to the development of semiconductor diode lasers and is currently researching the biophotonics applications of these lasers. In a semiconductor diode laser, the front and back surfaces of the diode form the resonant cavity that generates light emission when electrons and holes recombine at the p-n junction. Since the laser diode gain medium is relatively small compared to the wavelength of the laser light, the beam divergence of the laser output is relatively large. Thus diode lasers do not focus as well as other types of lasers. Semiconductor laser technology requires additional optical elements to provide a good quality focus of the laser beam. Moreover, the small size of semiconductor lasers provides efficient packaging. They can be operated on battery power and therefore are useful for remote operation. Some semiconductor lasers are tuneable over a broad wavelength range. High-power diode lasers are generally not tuneable; however, many wavelengths of interest are available for medical applications. Solid-state lasers are oftentimes tuneable and both types of lasers can be frequency shifted by non-linear optical techniques.

Although laser technology has made significant strides in recent years, a significant amount of work still needs to be done to develop the next generation of semiconductor lasers. Some of the more significant research efforts are directed at developing solutions for ultraviolet (UV)-blue-green lasers; increasing substrate stability; advancing high-power output; increasing reliability, coherence, and constant wave (CW) operation; finding more solutions in the mid-infrared; and developing compatible fiber optics.

The Directorate became involved in the biophotonics applications of semiconductor technology as a result of an Air Force Special Operations Command (AFSOC) mission need statement. The special operations community defined their requirements to be the development of lightweight, versatile equipment for special operations users in support of covert, clandestine, conventional, humanitarian, and civil military operations. AFSOC requested operation under high threat conditions to include rapid control and stabilization of bleeding, contaminated or infected ballistic and burn wounds, while at the same time meeting all the constraints of the AFSOC mission - severe environment, rechargeable, portable, and lightweight.

Since the Directorate's main objective was to support the warfighter and enhance combat casualty care capabilities, an aggregation of customers was developed. Some partners include the United States Special Operations Command, AFSOC, US Marine Corps Expeditionary Forces, US Army Combat Casualty Care Program, USAF Mobile Field Surgical Teams, Defense Advanced Research Projects Agency - Advanced Biomedical Technology, National Aeronautics and Space Administration, and the US Air Force Clinical Investigation Division.

Two systems developed for military needs were jointly known as the Field Medical Laser Systems (FMLS), but were individually named the Medpac and Medpen (Figure 1). The Medpac is comprised of a laser diode array at 808 nm with ten watts of output power. This eight-pound system is capable of cutting, coagulating, and closing. The second system, the Medpen, uses a laser diode array at 980 nm with five watts of output power. This system is also capable of cutting, coagulating, and closing, but weighs less than one pound. Researchers realized that this useful technology can be applied to a number of biophotonic applications and renamed the device the Portable Infrared Laser System (PIRLS).

Understanding laser tissue interactions is essential in defining the direction for the Directorate's biophotonics applications program. Diode lasers that operate between 0.6-1.0 μm seem to produce low scatter, lower water absorption, low protein absorption, and high hemoglobin absorption. All of these factors make diode laser wavelengths useful for many medical applications. Preliminary experiments demonstrated extremely rapid and efficient blood coagulation, which is probably due to the high hemoglobin absorption; however, diode laser wavelengths also apparently enhance photodynamic therapy. Diode lasers at other wavelengths can be used to investigate tissue interaction effects resulting from the different absorption and transmission properties for those wavelengths.

Because of the differences in absorption properties for various wavelengths (Figure 2), a number of different potential applications for semiconductor lasers exist. These other types of laser-tissue interactions include photocoagulation, photothermal ablation, and photochemical ablation. Other categories of potential medical applications include photodynamic therapy, thermotherapy, non-invasive surgery, minimally-invasive surgery, invasive surgery, and diagnostics and imaging. The Directorate's biophotonics applications program has research and development efforts in many of these areas.

In an effort to best leverage developmental funding, the Directorate focused significant resources on developing dual-use technology applications. Dual-use for the military implies both a military and civilian application for the particular product, which allows the military assistance in establishing viable commercial products and developing a source of supply for military products. Contractual mechanisms that allowed the Directorate to continue to pursue dual-use projects include the Small Business Innovative Research (SBIR) program, the Small Business Technology Transfer (STTR) program, and Cooperative Research and Development Agreements (CRADAs). Some specific projects in the Directorate's biophotonics applications of lasers program include:

SBIR program

- Cynosure, Inc. - Internal Hemostasis
- Star Medical - Burn Diagnostics
- Physical Sciences - Cancer Treatment & Monitoring
- SEA, Inc. - Wound Stabilization System
- Uniphase - 630 nm diode lasers for Medical Applications
- Sensors Unlimited - Medical Diagnostic System
- Deacon Research - Medical Diagnostic Microsensor

STTR program

- Fiberoptic Fabrication, Inc. - Treatment of Glaucoma
- Surgimedics/ESP Inc. - Wound Decontamination

CRADAs

- Indigo - Interstitial Thermotherapy for Benign Prostate Hyperplasia (BPH)
- Fiberoptic Fabrication, Inc. - PIRLS commercialization

The Directed Energy Directorate determined dual-use biophotonics applications of high-power diode laser and solid-state lasers to be a critically important technology focus area within the Directorate's technology transfer program. A significant program for cooperative projects in the area of biophotonics and medical applications of diode laser technology is continuing. Due to the enormous potential for portability, compactness, and their effective interaction with tissue, diode lasers will continue to be an exciting area of biophotonics applications research well into the 21st century.

Other contributing authors in this research include Alan H. Paxton, Chad Lindstrom and William T. Cooley of the Directed Energy Directorate.

This article was written by Dr. William P. Latham of the Air Force Research Laboratory's Directed Energy Directorate. For more information contact TECH CONNECT at 1-800-203-6451 or visit the web site at http://www.afrl.af.mil (Technology Transfer). Reference document DE-99-03.

FMLS
Medpac

SPECIFICATIONS

- Laser Diode Arrays
- 10 W of Output Power (808 nm)
- Capable of Cutting, Coagulating, & Closing

ACHIEVEMENTS

- Clinical, Field, Flight, and Chamber Tests
- NASA Field and Parabolic Flight Tests
- Final Report to HQ AFSOC, Conclusion of 6.3 Dem/Val Phase
- CRDA for further development and Commercialization

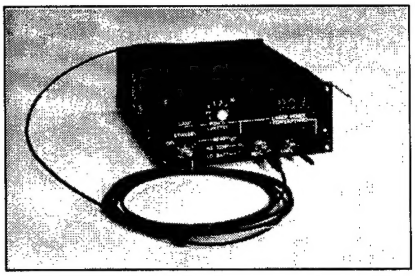

FMLS
Medpen

SPECIFICATIONS

- Laser Diode Arrays
- 5 Output Power (980 nm)
- Capable of Cutting, Coagulating, & Closing
- Mini-Medpen: 1 W fibered diode, free beam lasing

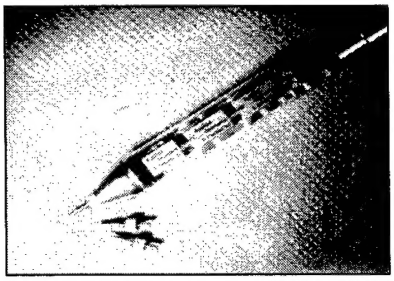

ACHIEVEMENTS

- Clinical, Field, Flight, and Chamber Tests
- NASA Field and Parabolic Flight Tests
- Final Report to HQ AFSOC, Conclusion of 6.3 Dem/Val Phase
- Investigation Laser Tissue Soldering with Mini-Medpen

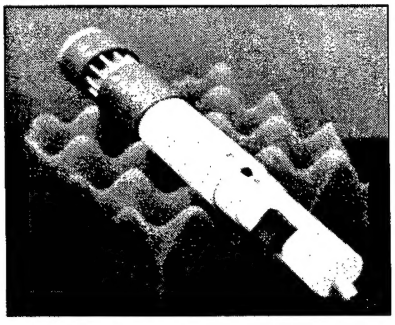

Figure 1. FMLS Medpac and FMLS Medpen.

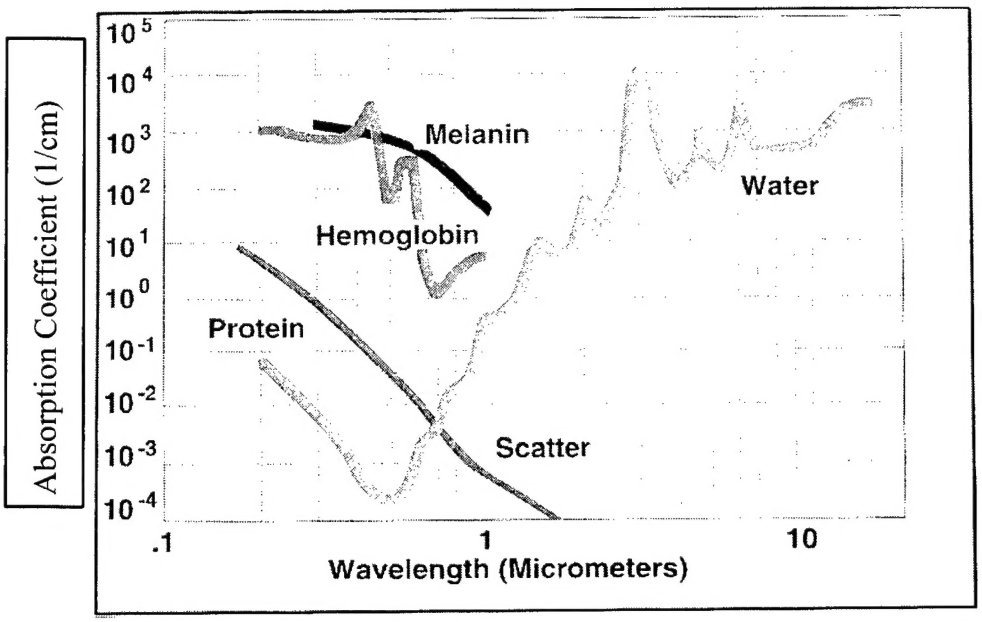

Figure 2. Tissue absorption coefficients for various wavelengths.